Pezzella *et al.*
Journal of Hematology & Oncology (2024) 17:127
https://doi.org/10.1186/s13045-024-01641-7

Journal of Hematology & Oncology

RESEARCH

Open Access

Tumor-derived G-CSF induces an immunosuppressive microenvironment in an osteosarcoma model, reducing response to CAR.GD2 T-cells

Michele Pezzella[1†], Concetta Quintarelli[1,2†], Maria C. Quadraccia[1,3], Andrea Sarcinelli[1,4], Simona Manni[1], Laura Iaffaldano[1], Alessio Ottaviani[1], Roselia Ciccone[1], Antonio Camera[1], Maria L. D'Amore[1], Stefano Di Cecca[1], Matilde Sinibaldi[1], Marika Guercio[1], Mariasole Aurigemma[1,3], Pamela De Falco[1], Valentina Fustaino[1], Rossella Rota[1], Silvia Pomella[1], Matteo Cassandri[1], Angela Di Giannatale[1], Chiara Agrati[5], Veronica Bordoni[5], Federica Guarracino[5], Michele Massa[1], Giada Del Baldo[1], Marco Becilli[1], Giuseppe M. Milano[1], Francesca Del Bufalo[1], Franco Locatelli[1,6*†] and Biagio De Angelis[1*†]

Abstract

Sarcomas are rare, mesenchymal tumors, representing about 10–15% of all childhood cancers. GD2 is a suitable target for chimeric antigen receptor (CAR) T-cell therapy due to its overexpression in several solid tumors. In this preclinical study, we investigated the potential use of iCasp9.2A.GD2.CAR-CD28.4–1BBζ (CAR.GD2) T-cells as a treatment option for patients who have GD2-positive sarcomas and we sought to identify factors shaping hostile tumor microenvironment in this setting. GD2 expression was evaluated by flow-cytometry on primary tumor biopsies of pediatric sarcoma patients. GD2 expression in sarcoma cells was also evaluated in response to an enhancer of zeste homolog 2 (EZH2) inhibitor (Tazemetostat). The antitumor activity of CAR.GD2 T-cells was evaluated both in vitro and in vivo preclinical models of orthotopic and/or metastatic soft-tissue and bone sarcomas. GD2 expression was detected in 55% of the primary tumors. Notably, the Osteosarcoma and Alveolar Rhabdomyosarcomas subtypes exhibited the highest GD2 expression levels, while Ewing sarcoma showed the lowest. CAR.GD2 T-cells show a significant tumor control both in vitro and in vivo models of GD2-expressing tumors. Pretreatment with an EZH2 inhibitor (Tazemetostat) upregulating GD2 expression, sensitizes $GD2^{dim}$ sarcoma cells to CAR.GD2 T-cells cytotoxic activity. Moreover, in mouse models of disseminated Rhabdomyosarcomas and orthotopic Osteosarcoma, CAR.GD2 T-cells showed both a vigorous anti-tumor activity and long-term persistence as compared to un-transduced T-cells. The presence of immunosuppressive murine myeloid-derived suppressor (MDSC) cells significantly reduces long-term anti-tumour activity of infused CAR.GD2 T-cells. Tumor-derived G-CSF was found to be one of the key factors driving expansion

[†]Michele Pezzella and Concetta Quintarelli: Co-first authors.

[†]Franco Locatelli and Biagio De Angelis: Co-last authors.

*Correspondence:
Franco Locatelli
franco.locatelli@opbg.net
Biagio De Angelis
biagio.deangelis@opbg.net
Full list of author information is available at the end of the article

© The Author(s) 2024. **Open Access** This article is licensed under a Creative Commons Attribution-NonCommercial-NoDerivatives 4.0 International License, which permits any non-commercial use, sharing, distribution and reproduction in any medium or format, as long as you give appropriate credit to the original author(s) and the source, provide a link to the Creative Commons licence, and indicate if you modified the licensed material. You do not have permission under this licence to share adapted material derived from this article or parts of it. The images or other third party material in this article are included in the article's Creative Commons licence, unless indicated otherwise in a credit line to the material. If material is not included in the article's Creative Commons licence and your intended use is not permitted by statutory regulation or exceeds the permitted use, you will need to obtain permission directly from the copyright holder. To view a copy of this licence, visit http://creativecommons.org/licenses/by-nc-nd/4.0/.

of immunosuppressive murine and human MDSC, thus indirectly limiting the efficacy of CAR.GD2 T-cells. Our preclinical data strongly suggest that CAR.GD2 T-cells hold promise as a potential therapeutic option for the treatment of patients with GD2-positive sarcomas. Strategies to tackle hostile immunosuppressive MDSC are desirable to optimize CAR.GD2 T-cell activity.

Keywords GD2, Chimeric antigen receptor (CAR), Sarcoma, ICasp9.2A.GD2.CAR-CD28.4–1BBζ, CAR.GD2 T-cells, EZH2 inhibitor, Myeloid-derived suppressor cells, CXCL8, G-CSF

Introduction

Sarcomas are rare mesenchymal neoplasia that include a variety of bone and soft-tissue tumors, affecting all ages; they are relatively more common in pediatric patients, accounting for 10–15% of childhood cancers [1].

In children and adolescents, the most common sarcomas include Osteosarcoma (OS), Rhabdomyosarcoma (RMS), Ewing's sarcoma (EWS) and the rare desmoplastic small round cell tumors (DSRCT), while leiomyosarcomas and liposarcomas, typically present in older patients [2]. Despite their rarity, sarcomas represent a significant cause of childhood mortality, accounting for approximately 13% of cancer-related deaths in individuals aged 0–19 years [3]. Furthermore, despite many efforts to identify targeted therapies, such as the utilization of tyrosine kinase inhibitors in the treatment of patients with soft-tissue and bone sarcomas, or the administration of intensive chemotherapy and/or radiation, followed by surgical intervention, clinical outcomes have not shown significant improvement over the last years for these patients. Thus, there is an urgent, unmet need to develop and validate novel treatment strategies to improve sarcoma patient outcomes [4].

Chimeric antigen receptor (CAR) T-cell immunotherapy stands out as one of the most promising approach for tumor treatment. Nevertheless, the identification of suitable antigens to target tumor cells is a crucial and challenging step in the successful development of CAR T-cell therapy for sarcomas.

Numerous antigens have been evaluated as potential target for adoptive therapy with CAR T-cells in sarcoma models, including alkaline phosphatase (ALP) in OS preclinical model [5], fibroblast growth factor receptor 4 (FGFR4) in RMS [6], and B7-H3 (CD276) in pediatric sarcoma [7]. However, to date, only few clinical trials employing CAR T-cells has been reported for sarcoma patients, targeting specifically HER2 antigen [8, 9], epidermal growth factor (EGFR), the cancer/testis antigen NY-ESO-1, B7-H3 antigen, glypican 3 (GPC3) [10] and, more recently, the disialoganglioside GD2 antigen [11].

Indeed, Kaczanowska et al. recently conducted a Phase I trial (NCT02107963) of GD2 CAR T-cells (GD2-CAR.OX40.28.z.iC9), demonstrating the feasibility and safety of the approach in children and young adults with OS and neuroblastoma (NBL). Despite the difference in the CAR design as compared to our own construct tested in NBL [12, 13], the performed correlative studies clearly showed the relevance of cytokine and myeloid cell signaling in influencing patient's response to CAR.GD2 T-cells and highly correlating with the transient clinical response observed [11].

GD2 is a tumor-associated carbohydrate antigen, reported to be overexpressed in several solid tumors, including NBL [14], melanoma [15], diffuse midline gliomas [16, 17], medulloblastoma [18], small cell lung cancer (SCLC) [19], breast cancer [20], retinoblastoma [21] and DSRCT [22], OS, EWS [23] and RMS [24]. The β−1,4-N-Acetyl-Galactosaminyltransferase 1 (B4GALNT1) gene encodes a key enzyme (GD2-synthase enzyme) that catalyzes the transfer of N-acetylgalactosamine into GM3 and GD3 via a beta-1,4 bond, resulting in the synthesis of GM2 and GD2 gangliosides. High B4GALNT1 expression is often associated to tumorigenesis and both the prognosis of multiple types of tumors [25] and the overexpression of the GD2 in tumor cells is linked to high expression of GD2-synthase enzyme [26].

GD2 is normally expressed during fetal development and is highly restricted to the central nervous system in healthy adults, with low levels of expression on peripheral nerves and skin melanocytes [27].

Recently, we carried out an academic phase I/II clinical trial using our academic, third-generation iCasp9.2A.GD2.CAR-CD28.4–1BBζ T-cells (hereafter CAR.GD2 T-cells), incorporating CD28 and 4-1BB as costimulatory domains and the suicide gene inducible caspase-9, as safety switch [12], to treat patients with relapsed/refractory and/or high-risk NBL (ClinicalTrials.gov Identifier: NCT03373097). A total of 27 children with heavily pretreated NBL were enrolled in the trial, seventeen children had a response to the treatment (overall response rate, 63%) [13]. Based on these outstanding results, we investigated if we could translate our therapeutic approach also to GD2 positive (GD2+) sarcoma patients and, thus, we focused our preclinical investigations to test the efficacy of CAR.GD2 T-cells, in the context of sarcoma tumours. We found that CAR.GD2 T-cells demonstrated significant cytotoxic activity against GD2-positive sarcoma cell lines, this effect being closely correlated to the level of

target antigen expression. In this context, the inhibition of Enhancer of zeste homolog 2 (EZH2) with Tazemetostat has been demonstrated to restore the expression of sialyltransferase GD3 synthase (GD3S; ST8SIA1), thereby potentially re-establishing GD2 expression in several cancers, including EWS [28], SCLC and non-SCLC (NSCLC) [29], NBL [30] and medulloblastoma [18]. Based on these findings, we aimed to investigate whether EZH2 inhibition could also effectively upregulate GD2 expression in RMS and OS cells, addressing the challenge of low GD2 expression in these malignancies. Lastly, we have also observed that tumor microenvironment (TME) is significantly shaped by soluble factors produced by sarcoma cells.

Tumor-derived CXCL8 was reported to be a potent chemotactic factor for neutrophils, myeloid-derived suppressor cells (MDSCs) and monocytes, which are considered immunosuppressive components in the TME [31].

In addition to these cell types, regulatory T-cells (Tregs) and tumor-associated macrophages (TAMs) also play significant roles in fostering an environment that impairs anti-tumor immunity. Collectively, these cells form a complex network that not only supports tumor growth and facilitates immune evasion, but may also negatively impact the therapeutic efficacy of CAR. GD2 T-cells. Addressing the interactions among cancer and these immunosuppressive components is essential for enhancing the effectiveness of immunotherapeutic strategies.

In the context of OS, CXCL8 and IL-6 mediate metastatic tropism of tumor cells to lung [31–33]. Granulocyte colony-stimulating factor (G-CSF) is a cytokine involved in maturation and mobilization of bone marrow neutrophils [34]. It has been reported to be a critical regulator of migration, proliferation and function of MDSCs in colitis-associated cancer [35]. Additionally, it fosters the long-term survival of tumor stem cells and contributes to the overall proliferation and migration of tumor cells [36].

In this work, we initially wondered if knockout of the CXCL8 gene in OS cell line could reduce murine immunosuppressive TME. Our preclinical xenograft mouse model of OS seems to exclude the direct involvement of CXCL8 in favoring the expansion of murine MDSC. Unexpectedly, only G-CSF was found to be directly involved in murine MDSC expansion in OS xenograft model. Additionally, it induced a notable expansion of human MDSC in in vitro models.

Overall, these findings contribute to better understanding the mechanisms underlying resistance to therapy and may help identify subgroups of sarcoma patients who are most likely to benefit from a therapeutic approach involving CAR.GD2 T-cells, considering the complexity of the tumor microenvironment and the challenges associated with overcoming immune suppression, especially in certain types of sarcomas.

Results

B4GALNT1 expression negatively affects overall survival of pediatric sarcoma patients

We initially performed a bioinformatic analysis, using the Xena Genome Browser exploration tool and examined multiple public databases, including TGCA and GTEX dataset, to explore mRNA expression of B4GALNT1 in solid tumors. This analysis revealed a significant overexpression of B4GALNT1 in various solid tumors, including bladder cancer, breast cancer, cholangiocarcinoma, colon adenocarcinoma, esophageal carcinoma, head & neck carcinoma, kidney clear cell carcinoma, liver hepatocellular carcinoma, lung adenocarcinoma, lung squamous carcinoma, NBL, paraganglioma and sarcoma, as compared to the healthy tissues ($p \leq 0.05$) (Fig. 1A). Based on these preliminary results, we further evaluated B4GALNT1 expression on Oncogenomic pediatric sarcoma dataset, TGCA and GTEX datasets, observing a significant GD2-synthase overexpression in OS patients' group, compared to healthy tissues (Fig. 1B). A correlation between high B4GALNT1 mRNA expression and reduced overall survival was found in OS ($p = 0.0002$) (Fig. 1C, left graph), RMS ($p = 0.036$) (Fig. 1C, middle graph) and EWS patients ($p = 0.025$) (Fig. 1C, right graph).

These findings underscore the potential role of B4GALNT1 as a prognostic biomarker in pediatric sarcomas, highlighting its relevance in the context of tumor progression and patient survival.

GD2 antigen is expressed with high variability in primary sarcoma biopsies

To investigate whether pediatric sarcoma could be a suitable target for CAR.GD2 T-cell therapy, we prospectively assessed GD2 expression on fresh tumor biopsies obtained from 64 sarcoma patients who were referred to our Institution. The flow-cytometry analysis conducted on the tumor tissues revealed positive expression of GD2 in 54.7% (35 out of 64) of the analyzed samples (Fig. 1D). When we stratified sarcoma samples according to their histotype, we found GD2 positivity in the following proportions: 54.5% (12/22) of OS patients; 85.7% (6/7) of alveolar RMS (ARMS) patients; 57.1% (8/14) of embryonal RMS (ERMS) patients, 33.3% (6/18) of EWS patients and 100% (3/3) of the DSRCT subgroup. The percentage of CD45 negative GD2 positive ($CD45^{neg}GD2+$) cells ranged from 1.4 to 92.3% in OS samples (average 17.2% ± 25.6%), from 1 to 70% in ARMS samples (average 28.8% ± 23.5%) and from 2 to

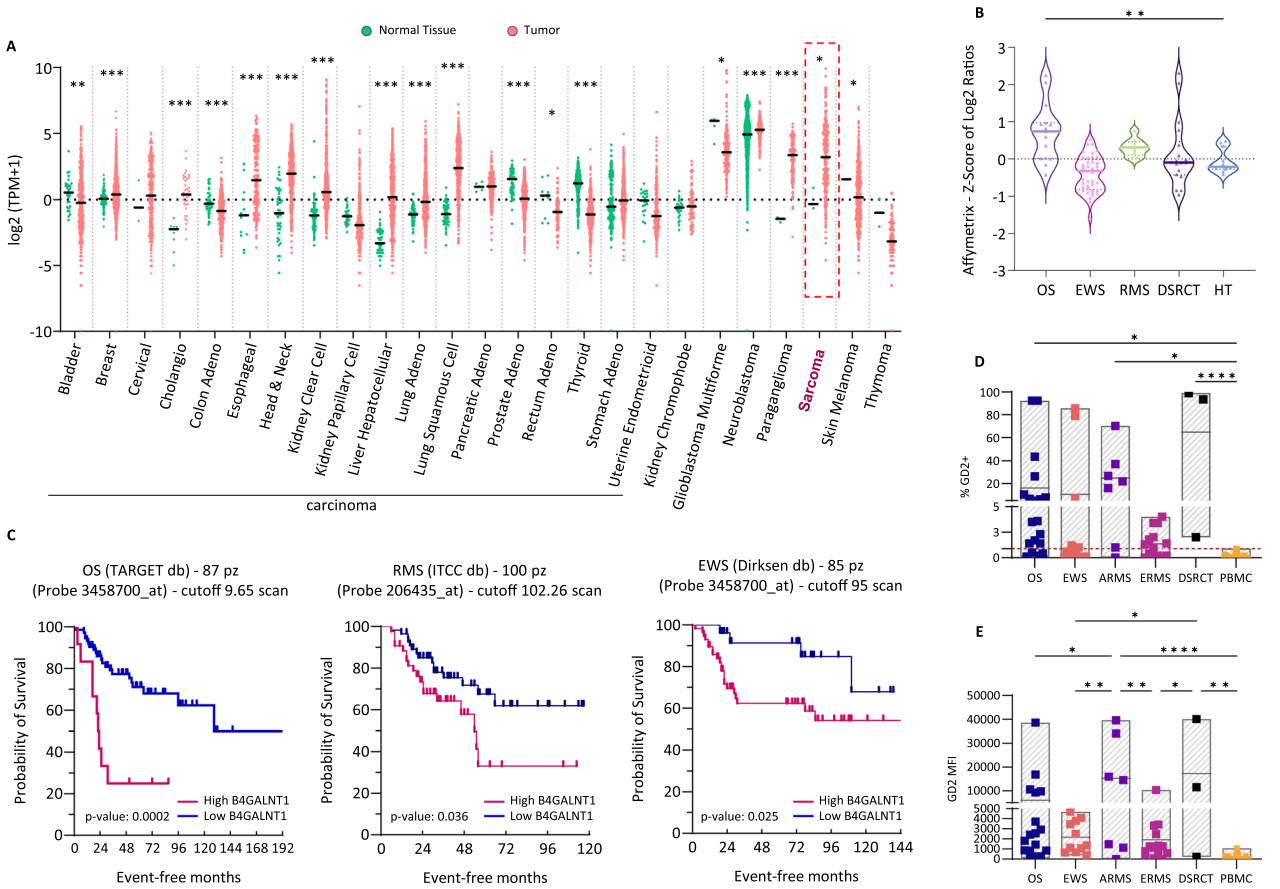

Fig. 1 GD2-synthase (B4GALNT1) mRNA gene expression profile in solid tumours. **A** Box plot depicting B4GALNT1 expression across cancers and healthy tissues. Data of TGCA and GTEX datasets showed expression level of B4GALNT1 in both normal tissues (green) and tumor patients with solid tumours (red). **B** B4GALNT1 expression on paediatric sarcoma cancer (Oncogenomics dataset—probe 206435_at) compared to Healthy Tissue (HT) control. **C** Kaplan–Meier analysis for overall survival in OS (TARGET dataset), RMS (ITCC dataset) and for Ewing's sarcoma (EWS) (Dirksen dataset) for B4GALNT1 mRNA expression. The percentage of GD2 positive cells **D** and GD2 MFI **E** on paediatric sarcoma tissues, evaluated by FACS analysis, compared to PBMC negative control. Two-way Anova was used as multi comparison test. *$p < 0.05$, **$p < 0.01$, ***$p < 0.001$, ****p-value = < 0.0001

99% in DSRCT (average 64.87% ± 49.07%). A lower percentage of CD45^{neg}GD2 + cells was detected in ERMS (average 2.3% ± 1.1%, range from 1.0 to 3.42%) and EWS sarcomas (average 15.0% ± 31.4%, range from 1 to 79%). As negative controls, we assessed the expression of GD2 on peripheral blood mononuclear cells (PBMC) from both sarcoma patients and/or healthy donors (GD2: 0.13% ± 0.28%). The gating strategy employed to identify GD2-positive cells in sarcoma patient biopsies is detailed in Supplemental Fig. 1A. Additionally, a representative FACS plot for both the bone and soft tissue sarcoma subgroups is presented in Supplemental Fig. 1B. The median fluorescence intensity (MFI) for GD2 expression was higher on tissue biopsies of OS (6,425 ± 9,810) and ARMS (17,785 ± 16,100), DSRCT (17,264 ± 20,537) than on those of EWS (1,972 ± 1,334), ERMS (2,319 ± 2982), or PBMC samples (128 ± 252) (Fig. 1E).

Overall, our findings indicate that a significant proportion of pediatric sarcomas express the GD2 antigen, although expression levels are highly variable. This underscores the importance of characterizing patient biopsies to assess potential eligibility for targeted therapy with CAR.GD2 T-cells.

GD2 antigen expression in human sarcoma cell lines recapitulates the variability found in primary samples.

To select the most relevant cellular models for sarcoma in which to test the activity of CAR T-cells targeting GD2, the expression of this target antigen was also assessed on 13 sarcoma cell lines, including MG-63, 143B, U-2OS, HOS and SAOS-2 (OS), RD and CT10 (ERMS), SCMC, RH4, RH41 and RH30 (ARMS), and A673 and SK-ES-1 (EWS) cell lines (Fig. 2 and Supplemental Fig. 2).

Among them, three cell lines showed high GD2 expression (i.e. a negligible, less than 3%, percentage of GD2 negative cells), such as MG-63, 143B, and U-2OS (Fig. 2A). In contrast, HOS (Fig. 2A), RD, CT10 (Fig. 2B), RH4, RH41, RH30 (Fig. 2C), A-673 and SK-ES-1 (Fig. 2D), exhibited a significant proportion of GD2-negative cells.

These findings highlight that the cellular sarcoma models applied in our study are able to recapitulate the variability in GD2 expression observed in the clinical setting.

CAR.GD2 T-cells eradicate GD2-positive sarcoma tumor cells in vitro

We aimed at evaluating the preclinical efficacy of targeting sarcoma tumors using third-generation CAR.GD2 T-cells, which incorporates the costimulatory domains of CD28 and 4.1BB and the suicide gene inducible caspase-9, as safety switch [12]. These gene-modified Tcells have been previously tested preclinically in NBL [12, 37, 38], H3K27M-mutated diffuse midline gliomas [17] and medulloblastoma [18] models. Additionally, CAR.GD2 T-cells have been already clinically validated in a phase I/II clinical trial for the treatment of patients with high-risk, relapsed/refractory NBL [13, 39].

In particular, in vitro antitumor activity of GD2.CAR T-cells on sarcoma tumor models was assessed by performing 5-day long-term co-culture assays, in a 1:1 Effector: Target (E:T) ratio using all sarcoma cell lines independently from GD2 expression (Fig. 2). As anticipated, CAR.GD2 T-cells completely eradicated all cell lines with high GD2 expression (i.e. cell lines with a negligible percentage of GD2 negative cells), such as MG-63, 143B, and U-2OS (Fig. 2A). In contrast, tumors with a significant proportion of GD2-negative cells, including

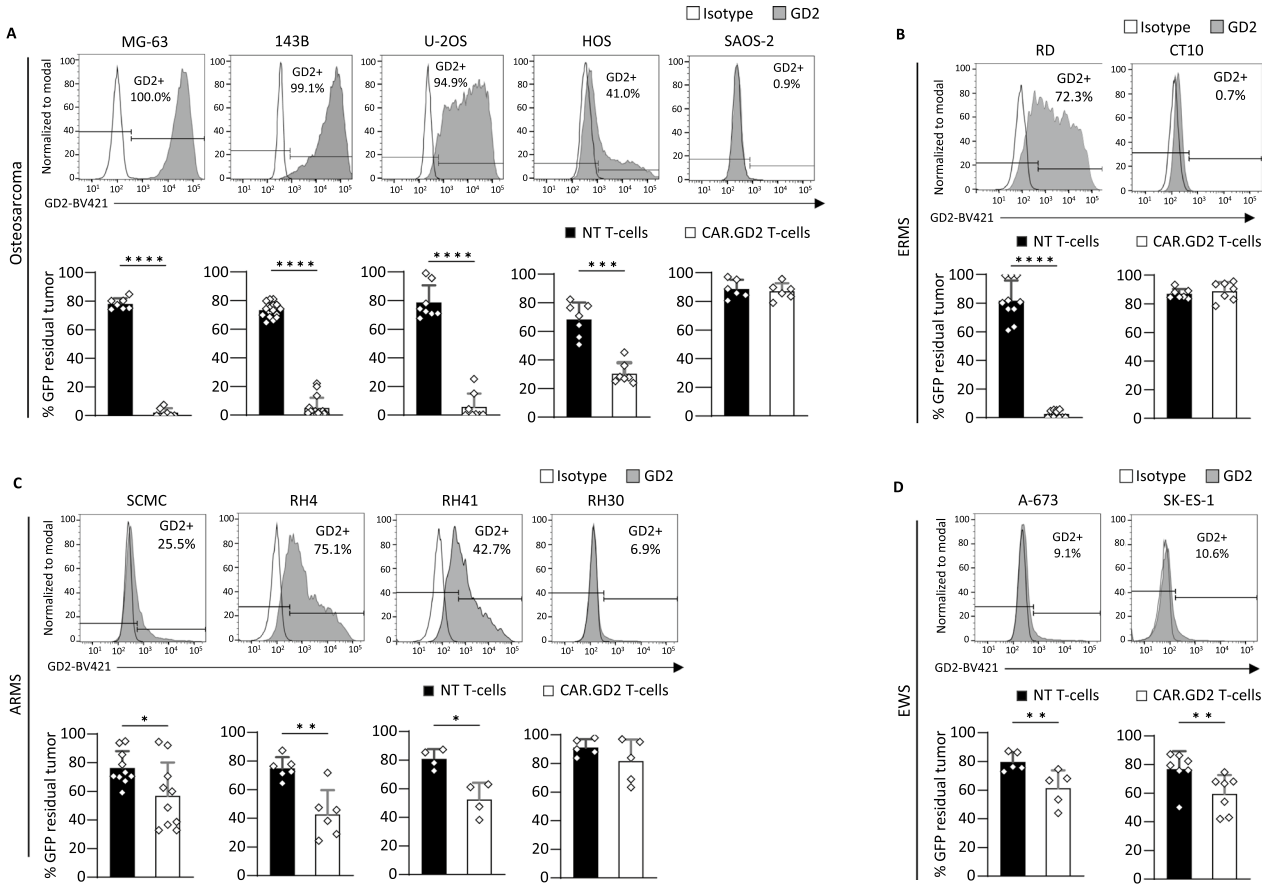

Fig. 2 In *vitro* anti-tumor activity of CAR.GD2 T-cells correlates to GD2 expression on human sarcoma cell lines. (**A**, top panel) Expression of GD2 in human osteosarcoma (OS) cell lines (143B, MG-63, U-2OS, HOS and SAOS-2); (**B,** top panel) in embryonal rhabdomyosarcoma (ERMS) cell lines (RD, CT10); (**C,** top panel) in ARMS cell lines (SCMC, RH4, RH41 and RH30); (**D,** top panel) in Ewing Sarcoma cell lines (SK-ES-1, A-673) as assessed by flow cytometry. The Isotype control was run for each tumor cell line (white). Five-day co-cultures were performed in 6 to 16 independent experiments, in which GFP + OS (**A,** bottom panel), ERMS (**B,** bottom panel) and ARMS (**C,** bottom panel), Ewing (**D,** bottom panel) cell lines were co-cultured with NT T or CAR.GD2 T-cells at the effector-target (E: T) ratio of 1:1. Paired t-Test was used as comparison test. *$p < 0.05$, **$p < 0.01$, ****p-value = < 0.0001

HOS (Fig. 2A), RH4, RH41 (Fig. 2C), A-673 and SK-ES-1 (Fig. 2D), exhibited only marginal control by CAR.GD2 T-cells. However, this tumor control was still statistically significant compared to the un-transduced (NT) T-cell condition. More in depth, in this last subgroup of sarcoma model, the residual tumor cells after the co-culture with CAR.GD2 T-cells were either GD2-negative or exhibited significantly lower GD2 mean fluorescence intensity (MFI) compared to control conditions (Supplemental Fig. 3A-D for RH4 model, and Supplemental Fig. 3E-H for HOS model). These finding highlight that, in cases of suboptimal GD2 expression, the use of targeted CAR T-cell therapy could result in the emergence of a GD2-negative tumor cell population.

Regarding RD cells, we observed an intriguing finding: despite a significant proportion of GD2-negative cells, this cell line was effectively controlled by CAR.GD2 T-cells (Fig. 2B). This unexpected result prompted us to further investigate this phenomenon. Specifically, we aimed at evaluating whether GD2 expression could be influenced by cell confluency. To this end, we seeded the cells in a 24-well plate at increasing densities (ranging from 100,000 to 250,000 cells/cm2) and collected the pellet for FACS analysis after 72 h. As shown in Supplemental Fig. 4A, the fraction of GD2-positive cells significantly increased with cell density, rising from 37.5% ± 7.2% to 75% ± 3.2% under the applied experimental conditions.

Lastly, we sought to determine whether pharmacological inhibition of EZH2 could positively modulate GD2 expression in sarcoma cells. As illustrated in Supplemental Fig. 4B, exposure of HOS, RH4, RH41, SCMC, and A673 cells to Tazemetostat for 7 days resulted in a significant upregulation of GD2 expression. Notably, this upregulation of the target antigen correlated with a marked increase in tumor control exerted by CAR.GD2 T-cells (Supplemental Fig. 4C).

As expected, the cytokine production strongly correlated with the killing activity of CAR.GD2 T-cells on sarcoma tumor cells (Supplemental Fig. 5). Indeed, significantly higher level of granzyme B (Supplemental Fig. 5A), IFN-γ (Supplemental Fig. 5B), IL2 (Supplemental Fig. 5C) and TNF-α (Supplemental Fig. 5D) cytokines were produced as compared to NT T-cells.

For the cell lines with high expression of GD2, namely 143B (OS) and RD (ERMS) cell lines, we decided to challenge further the system by applying different E:T ratio in both two-dimensional (2D) and three-dimensional (3D) culture models (Supplemental Fig. 6). Notably, CAR.GD2 T-cells demonstrated a significant and highly effective lysis of tumor cells even at a very low E:T ratio of 1:32 ($p = 0.0044$ for 143B and $p = 0.0130$ for RD cell line, respectively) in 2D models (Supplemental Fig. 6A-B). The robust antitumor efficacy of CAR.GD2 T-cells against both 143B and RD cell lines was validated also in 3D models using a real-time analysis (Supplemental Fig. 6C-D and Supplemental video 1 for 143B 3D models and—Supplemental video 2 for RD 3D model, respectively). Remarkably, already at 12 and 24 h from the starting of the co-culture, a substantial decrease in tumor spheroids was noted for both 143B ($p \leq 0.001$) and RD ($p \leq 0.001$) cell lines compared to control NT T-cells, across various E:T ratios (10:1, 5:1 and 1:1).

Importantly, we were also able to prove that CAR.GD2 T-cells were highly effective against primary tumor cells derived from a biopsy of an OS patient (Supplemental Fig. 7), exerting a significant cytotoxicity on tumor cells derived from a lung metastasis of a patient affected by OS (Supplemental Fig. 7A), with the eradication of GD2 + (CD3-) tumor cells and producing a significant level of IFN-γ (Supplemental Fig. 7B).

Overall, these findings highlight the potential of CAR.GD2 T-cells as a promising therapeutic strategy for targeting GD2-positive sarcomas, especially when combined with GD2 modulation strategies such as EZH2 inhibition, to overcome the issue of heterogeneity in GD2 expression.

CAR.GD2 T-cells modulate their memory profile in response to prolonged exposure to sarcoma cell lines

In the "stressed" co-culture experiments (Fig. 3), we evaluated the ability of CAR.GD2 T-cells, as compared to NT T-cells, to kill sarcoma cells in vitro after subjecting them to repeated exposures to RD (Fig. 3A-G) or 143B cell lines (Fig. 3H-N) (every 5 days for 4 times). At each time point, we evaluated the percentage of residual tumor cells, total T-cells and the phenotype of CAR.GD2 T-cells in terms of: CAR expression, CD4 + /CD8 + CAR + ratio and memory profile (Fig. 3 and Supplemental Fig. 8).

In the RD model, CAR.GD2 T-cells exhibited significant antitumor activity until the second round of tumor exposure compared to NT T-cells (the residual tumor cells at day + 10 was equal to 52.5% ± 18.0% for CAR.GD2 and 92.6% ± 3.4% for NT T-cells, ≤ 0.001; Fig. 3B). The percentage of residual T cells was significantly higher for CAR.GD2 T-cells at day + 5 and day + 10 of tumor re-challenging as compared to NT T-cells (Fig. 3C). Moreover, the percentage of CAR + cells remained stable overtime (Fig. 3D), with a significant enrichment of the CD8 + CAR + subpopulation (white bars) after the first tumor re-challenging (from 30.5% ± 9.6% at day 0 to 55.9% ± 15.4% at day + 5, $p = 0.02$) (Fig. 3E). The evaluation of CAR T-cell memory profile reveals a rapid decline in *naïve* compartment in both CAR.GD2 and NT T-cells. The variation of memory subpopulations in the control NT T-cells was only marginal, with a significant accumulation of

mature effector memory (TEM) and terminally differentiated effector memory cells re-expressing CD45RA (TEMRA), as well as a reduction in the *naïve* subpopulation and TCM cells in the last time-points (Fig. 3F). By contrast, the proportion of *naïve* CAR.GD2 T-cells significantly decreased from 52.4% ± 15.4% at day 0 to 7.9% ± 7.0% at day 5 ($p = 0.004$), with a significant enrichment of T Central Memory (TCM) and T Effector Memory (TEM) cells (Fig. 3G). A reduction of *naïve* CAR + T-cells (Supplemental Fig. 8 was observed in CD8 + CAR + compartments (Supplemental Fig. 8A-B), with the increase of TCM (at day5) and TEM (at the following time points) T cells compared to day 0 (Supplemental Fig. 8B).

For the 143B model of sarcoma (Fig. 3H), CAR.GD2 T-cells exhibited an efficient tumor control after every round of tumor exposure (residual tumor cells at day + 20 was 38.5% ± 14.2% for CAR.GD2 T-cells and 89.9% ± 4.0% for NT T-cells, p = 0.014) (Fig. 3I). It is noteworthy that, the percentage of residual T-cells was significant higher for CAR.GD2 T-cells in each tumor re-challenge compared to NT T-cells (Fig. 3K). Furthermore, CAR + T-cells remained stable overtime (Fig. 3K). Moreover, also in the OS model, we observed a significant expansion of the CD8 + CAR + subpopulation after the second tumor exposure [CD8 + CAR T-cells from 40.1% ± 14.0% at day 0 to 52.4% ± 10.5% at day + 10 ($p = 0.0421$) and 60.9% ± 10.9% at day + 20 ($p = 0.0460$) (Fig. 3L)]. The 143B OS tumor did not affect the memory profile of control NT T-cells (Fig. 3M), while the *naïve* compartment of CAR.GD2 T-cells (Fig. 3N), after 5 days of co-culture, rapidly decreased from 64.8% ± 11.7% to 5.2% ± 2.5% ($p = 0.03$), with a significant enrichment of both TCM (from 19.1% ± 4.2% to 54.6% ± 30.3%, $p = 0.036$) and TEM compartment (from 8.6% ± 4.8% to 32.9% ± 24.9%, $p = 0.015$).

With a split analysis for the CD4 + and CD8 + cells, we observed a reduction of naïve CAR + T-cells (S upplemental Fig. 8) in both compartments (Supplemental Fig. 8C-D), as well as a significant enrichment of TEM (Supplemental Fig. 8C-D).

Overall, the "stressed" co-culture experiments demonstrated that CAR.GD2 T-cells exhibit potent antitumor activity against sarcoma cell lines, effectively reducing tumor cell populations upon repeated exposures. Notably, CAR.GD2 T-cells underwent a marked shift in their memory profile, with a substantial decrease in the T-cell naïve compartment and an increase in TCM and TEM populations after tumor re-challenges.

CAR.GD2 T-cells are highly effective in an embryonal RMS xenograft mice model

We next assessed the in vivo CAR.GD2 T-cell antitumor activity in soft-tissue sarcoma xenograft mice model (Fig. 4 and Supplemental Fig. 9), implanting in NSG mice the aggressive metastatic embryonal RMS RD cells engineered with GFP-FF-Luc for the in vivo monitoring of tumor growth (Fig. 4A). At the tumor engraftment, i.e. when the tumor's bioluminescence was detectable and measurable by the IVIS imaging system, mice were randomized to receive either control NT-T-cells or CAR.GD2 T-cells. The bioluminescence in RMS tumor-bearing mice, treated with NT T-cells, rapidly increased up to three logs in less than 50 days (Fig. 4B-C and Supplemental Fig. 9A-B) and mice either died or were sacrificed due to morbidity. The macroscopic analysis in sacrificed mice showed large tumor masses with metastasis located preferentially in the kidney and liver. Median survival of RMS-tumor-bearing mice treated with CAR.GD2 T-cells was significantly longer (69.5 days) compared to mice treated with NT T-cells (50 days) ($p = 0.0413$; Fig. 4D). Although circulating T-cells in mice treated with NT

(See figure on next page.)

Fig. 3 Long-term tumor control of CAR.GD2 T-cells in an in vitro co-culture assay of RMS and OS models under "stressed" conditions. **A** The panel shows the experimental design of "stressed" co-culture. Residual GFP + RD cells **B** and CD3 positive cells **C** were quantified during the "stressed" co-culture with tumor addition every 5 days. **D** Percentage of CAR + T-cells was evaluated during the "stressed" co-culture by FACS analysis. In particular, data are shown at Day 0 (scattered bar histogram), referring to CAR + T cell percentage before co-culture with tumor cells, and at Day + 5 (white bars), Day + 10 (light grey bars), Day + 15 (dark grey bars) and Day + 20 (black bars) after tumor addiction. **E** The graph shows the modulation of the distribution of CD4 + and CD8 + subpopulations of CAR.GD2 T-cells before (day 0) and after RD tumor cell addition at day + 5, + 10, + 15 and + 20. Stacked bar graphs show the analysis of T *Naïve* (striped white bars), TCM (dark grey bars), TEM (light grey bars) and TEMRA (black bars) CD3 + subsets in the long-term "stressed" co-culture with NT T-cells **F** or CAR.GD2 T-cells **G.** The panel **H** shows the experimental design of "stressed" co-culture. Residual GFP + 143B cells **I** and CD3 positive cells **J** were quantified during the "stressed" co-culture with tumor addition every 5 days. **K** Percentage of CAR + T-cells expression was evaluated during the "stressed" co-culture by FACS analysis. In particular, data are shown at Day 0 (scattered bar histogram), referring to CAR + T cell percentage before co-culture with tumor cells, and at Day + 5 (white bars), Day + 10 (light grey bars), Day + 15 (dark grey bars) and Day + 20 (black bars) after tumor addiction. **L** The graph shows the modulation of the distribution of CD4 + and CD8 + subpopulations of CAR.GD2 T-cells before (day 0) and after RD tumor cell addition at day + 5, + 10, + 15 and + 20. Stacked bar graphs show the analysis of T *Naïve* (striped white bars), TCM (dark grey bars), TEM (light grey bars) and TEMRA (black bars) CD3 + subsets in the long-term "stressed" co-culture with NT T-cells **M** or CAR.GD2 T-cells **N**. Data from four healthy donors (HDs) are expressed as mean ± SED. T-test was applied for the analysis. **p*-value ≤ 0.05; ***p*-value ≤ 0.01; ****p*-value ≤ 0.001 and **** ≤ 0.0001.

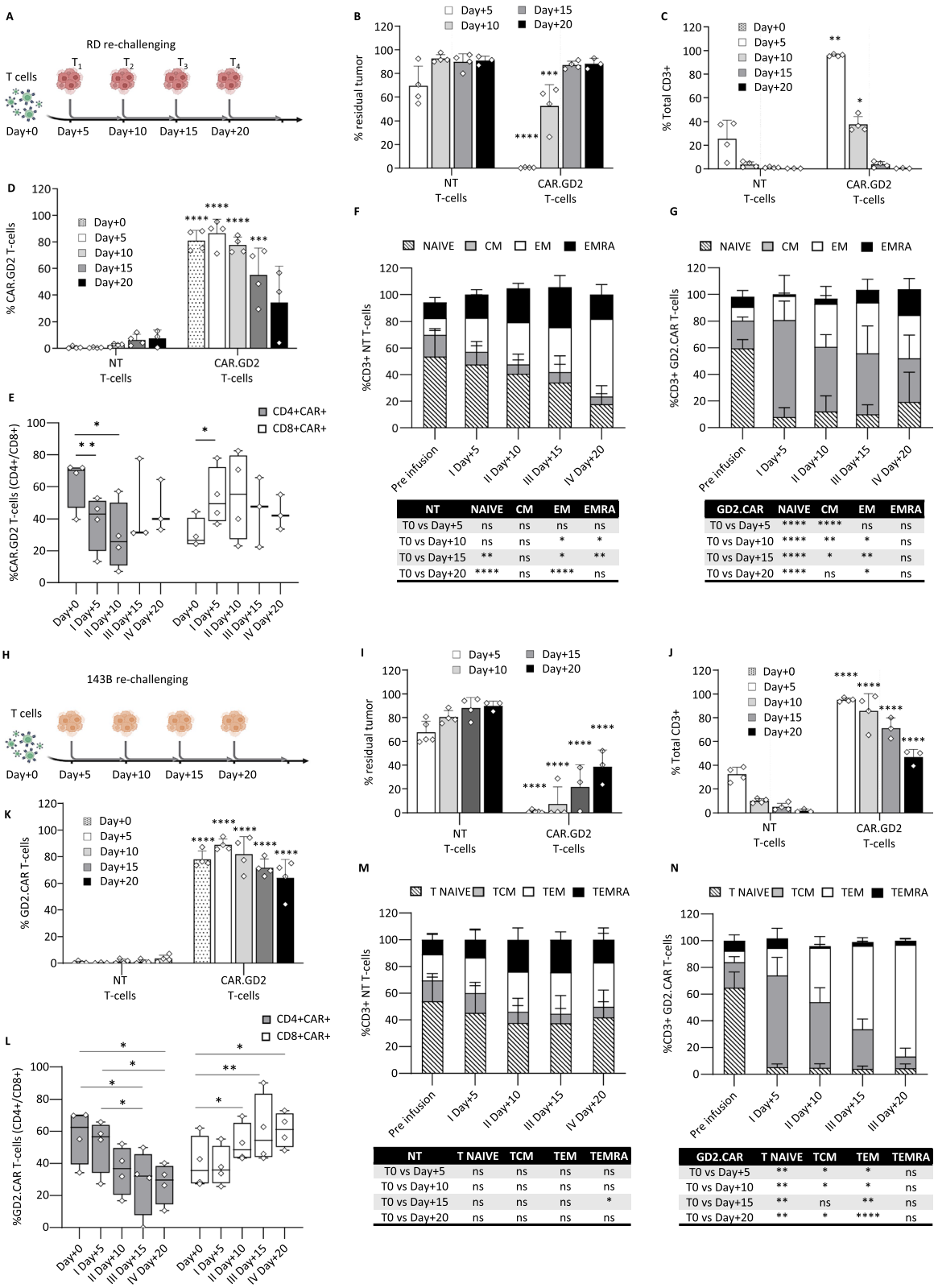

NT	NAIVE	CM	EM	EMRA
T0 vs Day+5	ns	ns	ns	ns
T0 vs Day+10	ns	ns	*	*
T0 vs Day+15	**	ns	*	**
T0 vs Day+20	****	ns	****	ns

GD2.CAR	NAIVE	CM	EM	EMRA
T0 vs Day+5	****	****	ns	ns
T0 vs Day+10	****	**	*	ns
T0 vs Day+15	****	*	**	ns
T0 vs Day+20	****	ns	*	ns

NT	T NAIVE	TCM	TEM	TEMRA
T0 vs Day+5	ns	ns	ns	ns
T0 vs Day+10	ns	ns	ns	ns
T0 vs Day+15	ns	ns	ns	*
T0 vs Day+20	ns	ns	ns	ns

GD2.CAR	T NAIVE	TCM	TEM	TEMRA
T0 vs Day+5	**	*	*	ns
T0 vs Day+10	**	*	*	ns
T0 vs Day+15	**	ns	**	ns
T0 vs Day+20	**	*	****	ns

Fig. 3 (See legend on previous page.)

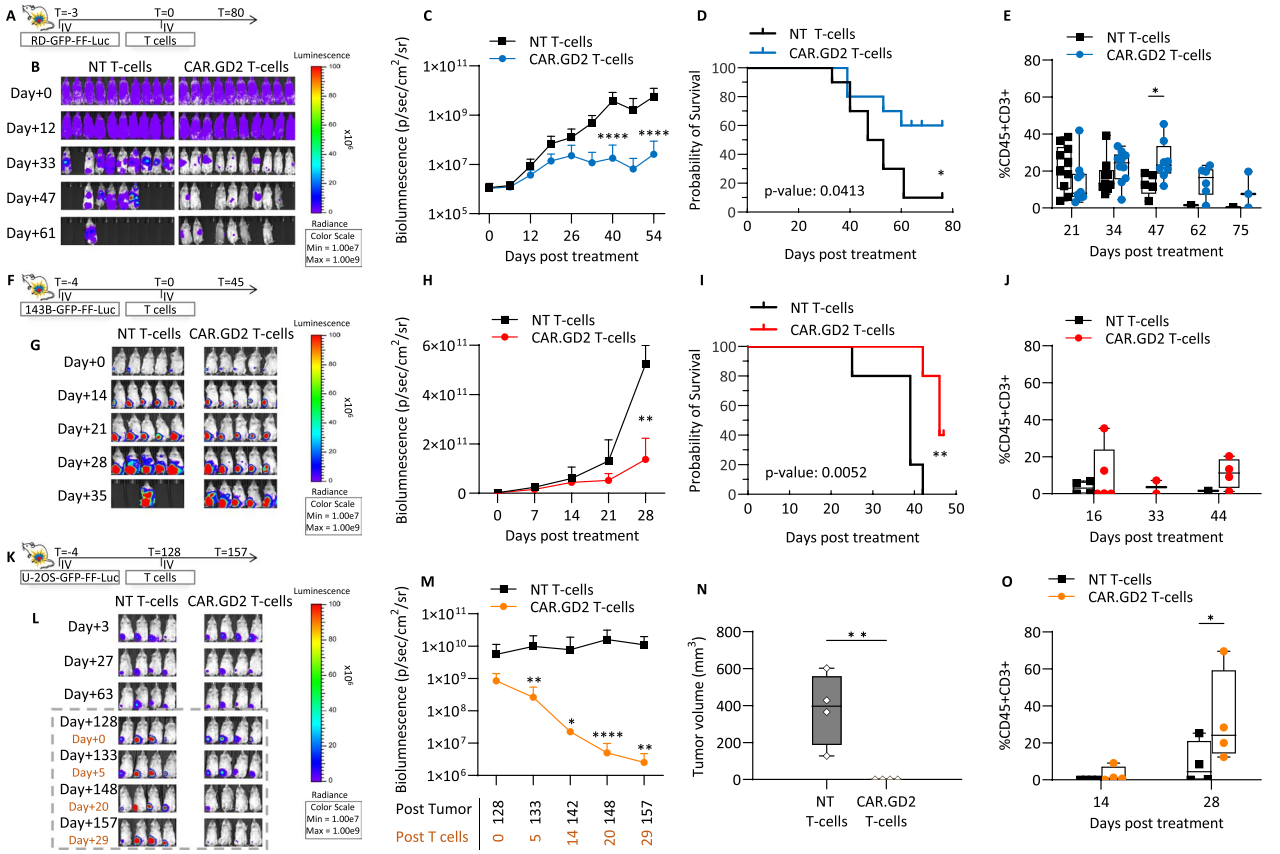

Fig. 4 In vivo experiments of NSG mice bearing GD2 + sarcoma cells (RD, 143B or U-2OS) treated with NT or CAR.GD2 T-cells. Experimental design (Figure created using Biorender—https://biorender.com) and in vivo bioluminescence imaging time-course of RD-GFP-FF-Luc tumor cells (**A**), 143B-GFP-FF-Luc (**F**) and U-2OS-GFP-FF-Luc (**K**) infused in NSG mice. At the time of tumor engraftment, 10^6 effector T-cells were administered through *i.v.* injection. The graph shows bioluminescence analysis of RD (ERMS) (**B, C**), 143B (OS) (**G, H**) and U-2OS (OS) (**L, M**) tumor-bearing mice model treated with NT T-cells (square symbol) or CAR.GD2 T-cells (dot symbol). Overall-Survival (OS) of RD (ERMS) (**D**) and 143B (OS) (**I**) tumor-bearing NSG mice treated with NT T-cells (black line) or CAR.GD2 T-cells (blue and red respectively). Two-way ANOVA was applied for the analysis. **p*-value ≤ 0.05; ***p*-value ≤ 0.01; ****p*-value ≤ 0.001 and **** ≤ 0.0001. (**N**) Explanted tumor-volume mass on sacrifice for NT T-cells and GD2.CAR T-cells mice group in U-2OS (OS) tumor model. Two-way ANOVA was applied for the analysis. **p*-value ≤ 0.05; ***p*-value ≤ 0.01; *** p-value ≤ 0.001 and **** ≤ 0.0001. Average of circulating human T-cells evaluated as % of CD45 + CD3 + (NT T-cells, square symbol) and CD3 + CAR + (CAR.GD2 T-cells dot symbol) until NSG-tumor bearing sacrifice for RD (ERMS) (**E**), 143B (OS) (**J**) and U2-OS (**O**) model. T-test and Two-way ANOVA was applied for the analysis. **p*-value ≤ 0.05; ***p*-value ≤ 0.01; ****p*-value ≤ 0.001 and **** ≤ 0.0001

T-cells were detectable during follow-up up to day + 47, they rapidly decreased and then disappeared (Fig. 4E). In contrast, in mice treated with CAR.GD2 T-cells, we observed a significant increase of circulating T-cells from 13.44% ± 11.60% at day + 21 to 25.48% ± 10.65% at day + 47 ($p = 0.04$) (Fig. 4E), with human T-cells as well as CAR + T-cells being detectable up to the last time-point of the experiment (day + 75; Supplemental Fig. 9C), suggesting a consistent CAR representation in the circulating T-cells over time (Supplemental Fig. 9C). During the experiment time-course, we observed a significant increase of the ratio between CD8 + and CD4 + T-cells compartment only for mice treated with CAR.GD2 T-cells (Supplemental Fig. 9D-E).

Our in vivo studies demonstrated that CAR.GD2 T-cells exert antitumor activity in a soft-tissue sarcoma xenograft model, significantly prolonging the survival of RMS tumor-bearing mice as compared to those receiving NT T-cells.

Efficacy of CAR.GD2 T-cell therapy in orthotopic mouse models of OS

To further corroborate our in vitro results, we evaluated the antitumor activity of CAR.GD2 T-cells in two distinct orthotopic mouse models of OS (Fig. 4F-O and Supplemental Fig. 10 and 11). In particular, in the first one, 143B-GFP-FF-Luc cells were orthotopically implanted in the tibia (Fig. 4F and Supplemental Fig. 10A). At tumour

engraftment, i.e. when the tumor's bioluminescence was detectable and measurable by IVIS imaging system, mice received either control NT-T-cells or CAR.GD2 T-cells. The in vivo data indicate that treatment with CAR.GD2 T-cells led to a significant decrease in tumour growth of the 143B cell line (Fig. 4G-H and Supplemental Fig. 10B). Additionally, the treatment with CAR.GD2 T-cells slightly improved the overall survival of the treated mice as compared to that of mice receiving NT T-cells, with a median survival of 46 days for CAR.GD2-T-cells compared to 39 days for NT T-cells ($p=0.0052$) (Fig. 4I). We observed a great expansion of human T-cells only in CAR.GD2 T-cells treated mice (Fig. 4J and Supplemental Fig. 10C), this highlighting that the engagement of the CAR by the target antigen was able to activate T cells, although their anti-tumor activity was suboptimal in the 143B OS model. Specifically, the percentage of circulating CAR.GD2-T-cells increased in the first month from 46.32% ± 19.81% to 61.72% ± 23.78% (day + 33) and remained stable up to day 44 (62.80% ± 17.54%) (Supplemental Fig. 10C) mice treated with NT T-cells, a significant enrichment of the CD4 + subpopulation was observed (Supplemental Fig. 10D, while we observed a similar distribution between CD4 + CAR + T-cells (53.8% ± 17.2%) and CD8 + CAR T-cells (43.0% ± 15.4%) in mice treated with CAR.GD2 T-cells at day + 33 post treatment (Supplemental Fig. 10D–E). Interestingly, the analysis of tumor mass for GD2 expression revealed that the residual tumor did not downregulate the expression of the target antigen (Supplemental Fig. 10F).

In the second orthotopic model of OS, we implanted in the tibia the less aggressive U-2OS-GFP-FF-Luc cell line, characterized by a slower growth rate in the mouse. As reported in Fig. 4K and Supplemental Fig. 11A, we obtained a robust engraftment of the tumor at day + 128 (compatible with a high tumor burden model, having a bioluminescence close to the saturating value of 1E10 p/s/cm^2/sr). Mice were then randomized to receive i.v. infusion of either NT T-cells or CAR T-cells. Tumor growth was monitored by IVIS imaging until day + 29 post-treatment (day + 155 post-tumor inoculation) (Fig. 4L); we observed a significant tumor regression in all CAR.GD2 T-cells treated mice compared control NT T-cells mice group (Fig. 4M). The difference in bioluminescence intensity was statistically significant since day 5 post CAR.GD2 T-cells infusion compared to the NT T-cell-mice group (Fig. 4M and Supplemental Fig. 11B). On the day of mouse sacrifice, the tumor volumes were assessed using a caliper. The results showed a complete absence of tumors in mice treated with CAR.GD2 T-cells as compared to the animals treated with NT T-cells where the mean value was 304.9 mm^3 ± 240.9 mm^3, $p \leq 0.01$ (Fig. 4N).

In CAR.GD2 T-cells treated mice, on day + 28, we observed a significantly higher number of T-cells, as compared to mice infused with NT T-cell (Fig. 4O), that persisted overtime (Supplemental Fig. 11C). Notably, as seen for the RMS model, we observed a significant reduction of the CD4 + CAR + T-cells subset and an enrichment of CD8 + CAR + T-cells (Supplemental Fig. 11D–E).

Altogether, these findings from both OS orthotopic mouse models reveal distinct responses to CAR.GD2 T cells: while treatment with CAR.GD2 T cells only reduced tumor growth in the aggressive 143B model, it induced notable tumor regression and complete tumor eradication in the less aggressive U-2OS model, highlighting the differential efficacy of CAR.GD2 T cells in varying OS contexts.

Expansion of murine MDSCs is restricted to 143B OS xenografts murine model and it is related to G-CSF.

It has been recently reported that the xenograft OS model of 143B induces a substantial expansion of both monocytic and polymorphonuclear (PMN) inhibitory murine MDSC [40]. Therefore, we decided to evaluate whether other OS lines and/or the RD ERMS line had the same immunomodulating effect. For this purpose, 143B, U-2OS, SAOS-2, MG-63 and HOS cell lines were orthotopically inoculated in the right tibia of NSG mice. For the ERMS model, the RD cell line was orthotopically inoculated in the right paw muscle of NSG mice (Fig. 5). The tumour bioluminescence was assessed weekly until tumour signal reached ≥ 1E + 9 p/s/cm^2/sr; at that point, mice were sacrificed (Fig. 5A). A non-tumour bearing NSG mice were also included for comparative analysis and considered as negative control. Circulating monocytic MDSC were evaluated weekly (from day + 7) in peripheral blood of mice included in the study, by FACS analysis, as previously reported [40] enumerating the absolute number of murine monocytic (CD11b + Ly6C +) (Fig. 5B) and PMN (CD11b + Ly6G + Ly6C–) MDSC (Fig. 5C). Starting from day + 14, there was a significant increase in both CD11b + Ly6G + and CD11b + Ly6C + MDSC only in NSG mice bearing the 143B tumor, but not in U-2OS, SAOS-2, MG-63, HOS, and RD tumor bearing mice or in non-tumor-bearing mice (Fig. 5B-C).

To investigate which 143B-secreted-chemokines could be determinant to induce a significant expansion of murine MDSC, we performed a differential secretome profile analysis by Luminex assays (Fig. 5D) evaluating 22 human cytokines/chemokines potentially involved in expansion and/or recruitment of MDSC at tumor site [41–43].

Culture media of 143B, U-2OS, MG-63, HOS, SAOS, RD cell lines were comparatively analyzed at 72 h from

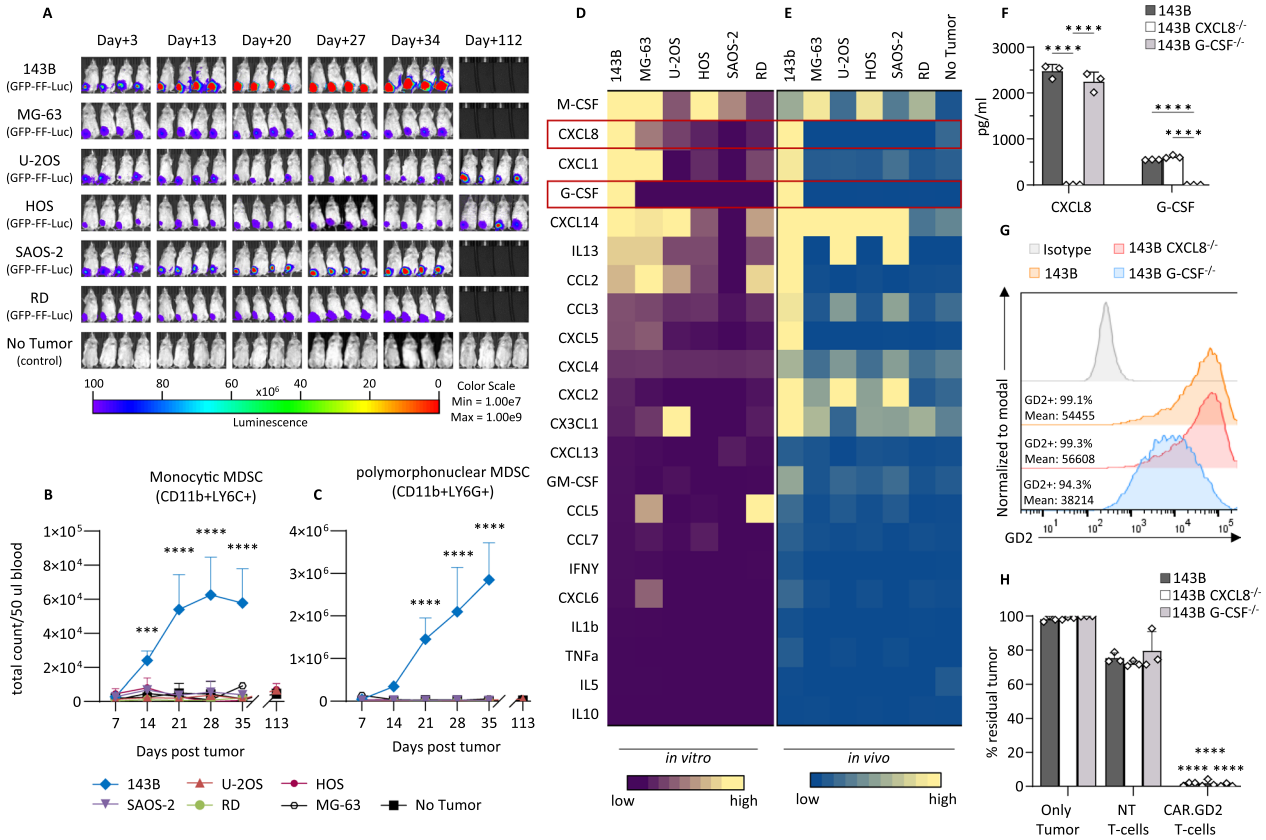

Fig. 5 Only the human OS 143B line, when implanted in NSG mice, induces the expansion of murine MDSCs. **A** NSG mice were engrafted with six different human sarcoma cell lines. Tumor growth was evaluated by In vivo imaging system (IVIS) for five different orthotopically models (200'000 cell/mice) of five OS cell lines (143B, U-2OS, SAOS-2, MG-63, HOS) and one ERMS cell line (RD). No tumor bearing mice have been used as control group. **B** Weekly plasma samples were collected from each tumor-bearing mouse and control mice, to investigate circulating mMDSCs using FACS flow-cytometry. The analysis looked for both monocytic MDSCs **B** and polymorphonuclear (PMN) MDSCs (**C**) cell subset of CD11b + cells. To ensure accurate comparison and data normalization across samples, counting beads were utilized. **p*-value = < 0.05; ***p*-value = < 0.01; ****p*-value = < 0.001; *****p*-value = < 0.0001, t test. **D-E** Quantitative analysis of multiple MSDC ligands was performed using the Luminex assay. Supernatant from tumor cultures (143B, MG-63, U-2OS, HOS, SAOS-2 and RD) **D** and plasma samples of tumor bearing mice (143B, MG-63, U-2OS,, HOS, SAOS-2 and RD) **E** were explored using a predesigned panel assay, at 72 h of culture and at time of mice sacrifice respectively. Quantification of the specified cytokines, including CCL2, CCL3, CCL5, CCL7, CX3CL1, CXCL1, CXCL2, CXCL4, CXCL5, CXCL6, CXCL8 (IL8), CXCL13, CXCL14, G-CSF (CSF3), GM-CSF, IFN-gamma, IL10, IL13, IL1b, IL5, MCSF, and TNF-alpha, was normalized on blank control background for the in vitro data (in violet) and no tumor sample for the in vivo data (in blu), and values reported in a Heatmap graph. Data are represented as mean ± standard deviation (SD) from n = 3. **F** The efficiency of CSF3 and CXCL8 KO in 143B cell lines was assessed by ELLA assay on 72 h cell lines supernatants. (**G**) Comparative Analysis of Crisped 143B OS Cell Lines for CXCL8 and G-CSF3 (CSF3). The cell lines 143B (wild-type control, orange line), 143B CXCL8$^{-/-}$ (143B CXCL8 knockout, red line), and 143B G-CSF$^{-/-}$ (143B G-CSF knockout, blue line), where analyzed for GD2 expression (percentage and GD2 MFI) by flow-cytometry and normalized on the Isotype Control. **H** The 143B wild-type control (dark grey), 143B CXCL8$^{-/-}$ (white), 143B G-CSF$^{-/-}$ (light gray) cells were co-cultured for 5 days with NT or GD2.CAR T-cells at E: T = 1:1 ratio. At the endpoint the percentage of residual tumor was evaluated by FACS as measure of GFP tumor expression. Data are expressed as mean ± SD from 3 donor. Statistical significance was determined using ANOVA test with **p* < 0.05, ***p* ≤ 0.01, ****p* ≤ 0.001, *****p* ≤ 0.0001

cell plating (Fig. 5D), while plasma derived from orthotopic mouse models was collected when tumor bioluminescent signal reach 10E6 p/s/cm^2/sr (Fig. 5E). In parallel, we also collected plasma from non-tumor-bearing mice, as negative control. As detailed in the heat-map, in both in vitro and in vivo models, the 143B tumor showed a higher production of G-CSF (for in vitro model: 555.55 pg/ml ± 0.34 pg/ml; and in vivo *model*: 3917.96 pg/ml ± 992.19 pg/ml) and CXCL8 (for in vitro model: 2560.42 pg/ml ± 26.15 pg/ml; and in vivo *model*: 3633.04 pg/ml ± 1951.73 pg/ml), as compared the other sarcoma cell lines, this finding supporting the potential involvement of these cytokines in murine MDSCs expansion [44] (Fig. 5D-E). To further investigate the role of these two cytokines, we knocked-out in 143B cells either CSF3 (G-CSF) or IL-8 (CXCL8) gene using

the CRISPR-Cas9 technology. The efficiency of G-CSF and CXCL8 knock-out in 143B cell lines was confirmed by ELLA assay on culture supernatants collected after 72 h of cell seeding (Fig. 5F). Both knocked-out 143B cell lines showed a similar GD2 expression in terms of both percentage and MFI level (Fig. 5G), this indicating that silencing of these two genes did not alter the expression of the GD2 target antigen. Moreover, we demonstrated that CAR.GD2 T-cells had a similar in vitro capacity to eradicate wild-type 143B cells, G-CSF$^{-/-}$ 143B or CXCL8$^{-/-}$ 143B cells (Fig. 5H). We then moved to develop the in vivo orthotopic model (Fig. 6A-B) implanting in the right tibia of NSG mice the 143B wild-type (orange line), 143B CXCL8$^{-/-}$ (red line), or 143B G-CSF$^{-/-}$ (blue line) cell line. Tumor growth did not significantly differ across the aforementioned cell models. Nevertheless, among the three animal models, only mice bearing 143B G-CSF$^{-/-}$ did not show the expansion of monocytic MDSC (231.26 ± 48.08 cells/100 µl blood) or PMN MDSC (1192.76 ± 237.54 cells/100 µl blood), their absolute number being comparable to that observed in control non-tumour-bearing NSG mice (monocytic MDSC:277.60 ± 59.74 cells/100 µl blood; and PMN-MDSC: 1381.96 ± 379.64 cells/100 µl blood, respectively, p = n.s.) (Fig. 6C-D). In contrast to the 143B G-CSF$^{-/-}$ model, mice bearing the 143B CXCL8$^{-/-}$ cell line exhibited high level of circulating monocytic MDSC (2278.36 ± 306.32 cells/100 µl blood) and PMN-MDSC (47,964.88 ± 8159.04 cells/100 µl blood), which were comparable to those found in 143B wild-type-bearing mice (monocytic MDSC: 2303.96 ± 317.70 cells/100 µl blood and PMN-MDSC: 39192.84 ± 9136.02 cells/100 µl blood; p = n.s.). To confirm the successful generation of human 143B KO xenograft models, plasma was collected from murine blood samples, and human cytokines were analyzed using a Luminex assay to assess the

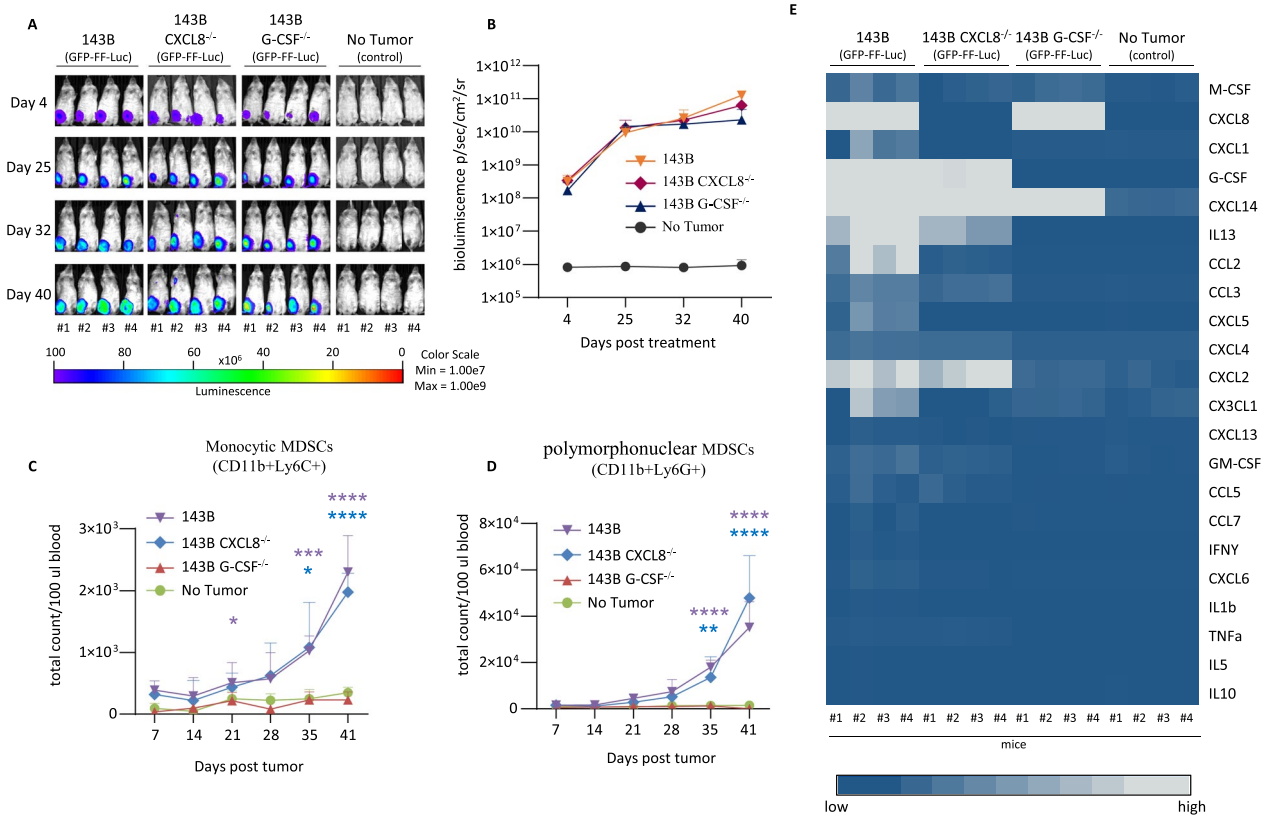

Fig. 6 Study of tumor secretome profile and MDSC investigation on sarcoma cell lines. **A** NSG mice were engrafted with three different human sarcoma cell lines (WT, Crisped 14B OS Cell Lines for CXCL8 and G-CSF3). **B** Tumor growth was evaluated by In vivo imaging system (IVIS) for all three different orthotopically models (200'000 cell/mice). No tumor bearing mice have been used as control group. Weekly plasma samples were collected from each tumor-bearing mouse and control mice, to investigate circulating mMDSCs using FACS flow-cytometry. The analysis evaluated both monocytic MDSCs **C** and polymorphonuclear MDSCs **D** cell subset of CD11b + cells. To ensure accurate comparison and data normalization across samples, counting beads were utilized. **p*-value = < 0.05; ***p*-value = < 0.01; ****p*-value = < 0.001; *****p*-value = < 0.0001, t test. **E** Quantification of the specified cytokines, including CCL2, CCL3, CCL5, CCL7, CX3CL1, CXCL1, CXCL2, CXCL4, CXCL5, CXCL6, CXCL8 (IL8), CXCL13, CXCL14, G-CSF (CSF3), GM-CSF, IFN-gamma, IL10, IL13, IL1b, IL5, MCSF, and TNF-alpha, was normalized on blank control background for the in vivo data, and single values reported in a Heatmap graph. Two-way Anova was used as multi comparison test. *$p < 0.05$, **$p < 0.01$, ***$p < 0.001$

expression of 22 human cytokines/chemokines, including G-CSF and CXCL8 in both 143B KO mouse models (Fig. 6E). As indicated in this panel, the production of G-CSF and CXCL8 was negligible in 143B KO xenograft mouse model. Altogether, our experimental results provide strong evidence that tumor-derived G-CSF, but not CXCL8, induces robust expansion of both monocytic and PMN-MDSCs in the xenograft NSG mouse model. To support the hypothesis that G-CSF secretion is primarily tumor-derived rather than a result of T-cell activation, we directly stimulated CAR.GD2 T cells with the 1A7 anti-idiotypic antibody, which functionally mimics the tumor-associated antigen disialoganglioside GD2. We evaluated G-CSF production after 24 h of stimulation (Supplemental Fig. 12). Our results showed no significant levels of G-CSF in either condition (NT T cells and CAR.GD2 T cells) (Supplemental Fig. 12A). This finding aligns with the behavior of other cytokines, such as IL-6 (Supplemental Fig. 12B) and IL-10 (Supplemental Fig. 12C), which are known to drive toxicity after CAR T-cell activation but are not directly produced by CAR T cells. Additionally, we assessed GM-CSF and IFNγ levels as positive controls (Supplemental Fig. 12D-E).

In summary, our findings demonstrate that tumor-derived G-CSF is primarily responsible for the robust expansion of both monocytic and PMN-MDSCs in the xenograft OS NSG mouse model, highlighting the significant indirect immunomodulatory role of G-CSF in the sarcoma microenvironment.

143B cell line drives a robust expansion/differentiation of human suppressive MDSC

To corroborate our data in a human setting, we set up different in vitro experimental approaches, summarized in Supplementary Fig. 13. First, PBMC from healthy subjects were directly co-cultured with 143B, 143B G-CSF$^{-/-}$, 143B CXCL8$^{-/-}$ and U-2OS cell lines (Fig. 7A) or with their conditioned medium (CM1, Fig. 7B), and the frequency of MDSC was evaluated by flow-cytometry before (day 0) and after three days of culture (day + 3). The gating strategy for the identification of early-MDSC (e-MDSC, CD14negCD15neg), monocytic-MDSC (Mo-MDSC, CD14posCD15neg) and polymorphonuclear-MDSC (PMN-MDSC, CD14negCD15pos) is described in Supplementary Fig. 14A-C.

We observed a significant reduction of the e-MDSC frequency at day + 3 in co-culture experiments with 143B and 143B G-CSF$^{-/-}$ and 143B CXCL8$^{-/-}$ cell lines, with a parallel significant increase of the frequency of Mo-MDSC, suggesting an OS-mediated differentiation toward Mo-MDSC (Supplementary Fig. 14D). Moreover, the analysis of the absolute numbers of the different MDSC subsets in co-culture assays demonstrated a significant expansion of PMN-MDSC after co-culture with 143B and U-2OS cell lines, and a significant expansion of Mo-MDSC after co-culture with 143B, 143B G-CSF$^{-/-}$ and 143B CXCL8$^{-/-}$ cells (Fig. 7C). In order to dissect the involvement of soluble mediators released by OS lines, we performed similar experiments using CM1 derived from 143B, 143B G-CSF$^{-/-}$, 143B CXCL8$^{-/-}$ and U-2OS cell lines.

Results showed that only 143B and 143B CXCL8$^{-/-}$ CM1 were able to induce a significant increase in the frequency and in the absolute number of Mo-MDSCs (Supplementary Fig. 14E and Fig. 7D, respectively). This finding suggests a crucial role of G-CSF but not of CXCL8, in driving a remarkable expansion of human Mo-MDSC subpopulation. To support the hypothesis that G-CSF plays a crucial role in inducing a robust expansion of Mo-MDSC from PBMC, we co-cultured freshly isolated PBMC with 143B G-CSF$^{-/-}$ cells, both with and without the addition of G-CSF at concentrations ranging from 0.5 to 50 ng/ml for 72 h (see Supplementary Fig. 15A). The introduction of G-CSF into the co-culture significantly promoted the expansion of Mo-MDSC (Supplementary Fig. 15B). In contrast, no expansion of Mo-MDSC was observed in G-CSF-treated PBMC alone (Supplementary Fig. 15C), indicating that other factors released by the 143B G-CSF$^{-/-}$ cells contribute significantly to the observed Mo-MDSC expansion.

Finally, we assessed the immunosuppressive effects of all conditioned media from OS (CM1) and from OS/PBMC cell lines (CM2, CM3 and CM4) in CAR.GD2 T-cells/OS co-culture killing assay (Fig. 7E). The CAR.GD2 T cell killing activity was monitored by Incucyte live cell imaging system for 5 days, and residual tumour-associated GFP confluence quantified overtime. CM1 from all OS lines did not have any direct suppressive effect on CAR.GD2 T-cells activity (black lines in Fig. 7E). Of note, CM2 and CM4 derived from 143B or 143B CXCL8$^{-/-}$ significantly reduced CAR.GD2 T-cell function (purple and blue lines respectively in Fig. 7E). In contrast, CM2 and CM4 derived from 143B G-CSF-/- and U-2OS did not have any suppressive effect on the antitumor activity of CAR.GD2 T-cells (Fig. 7E).

Overall, these findings underscore the critical role of tumor-derived G-CSF in promoting the expansion of immunosuppressive MDSCs.

Discussion

Numerous clinical studies have demonstrated promising results with the use of gene-modified CAR T-cell therapies in the treatment of hematological malignancies [45, 46], and more recently in solid tumors, including neuroblastoma [13] and H3K27M-mutated diffuse midline gliomas [16]. However, no significant clinical

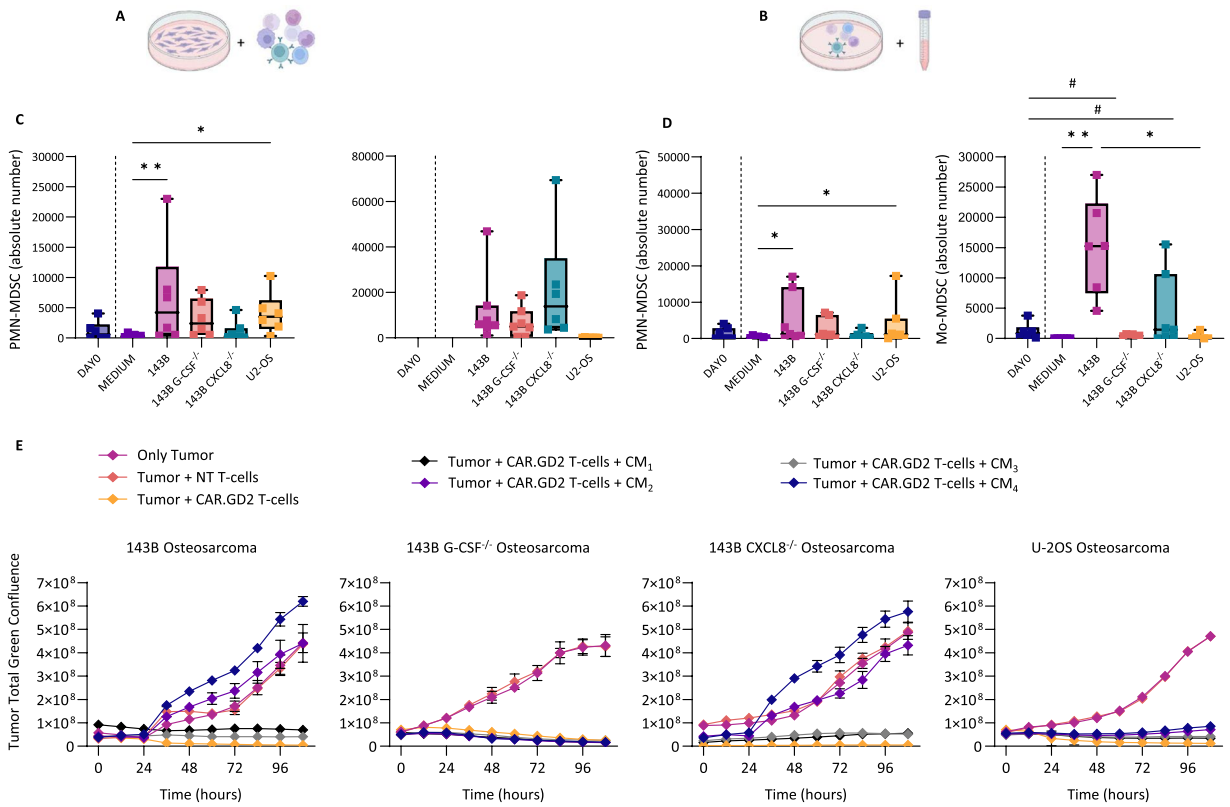

Fig. 7 OS 143B cells induce human Mo-MDSC expansion. Schematic representation of PBMC co-cultured with OS tumor cells (**A**) or with OS conditioned medium (CM) for 72 h (**B**). The absolute number of PMN-MDSC (left side panel), or Mo-MDSC (right side panel) before (day 0) and after three days of cell–cell contact (**C**) and cell-free experiments (**D**) with medium and OS cell lines. Results are shown as box and whiskers graphs showing all points. Friedman matched paired test was applied to compare different cell culture conditions, while Wilcoxon matched-pairs signed-rank test was used for group's comparison with respect to the absolute number quantified before culture (day0); p values are indicated in the graphs *#: $p < 0.05$. (**E**) Co-culture assay with all conditioned medium of OS/PBMC culture was real-time monitored by Incucyte live cell system imaging for five days to assess the tumor clearance by CAR.GD2 T-cells. Total green Confluence associated to the OS tumor cell lines was quantified overtime as a measure of residual tumor. Figure created using Biorender—https://biorender.com. Two-way ANOVA was applied for the analysis. *p-value ≤ 0.05; **p-value ≤ 0.01; ***p-value ≤ 0.001 and **** ≤ 0.0001

responses have been reported for sarcomas treated with CAR T-cells [11], highlighting the need to identify effective strategies for these patients. Indeed, the mechanisms associated with CAR-T cell efficacy are not yet fully understood, and the interaction between the TME and CAR T-cell therapy is considered a key factor that could directly influence CAR T-cell behavior and fate [47].

GD2, a tumor-associated disialoganglioside antigen, is an ideal target for CAR T-cell therapies because it is overexpressed in various solid tumors, while being minimally expressed on healthy tissues. Tumors positive for GD2 include pediatric embryonal tumors and several adult cancers. In this study, we provided evidence that the expression of B4GALNT1 (a GD2-synthase) is significantly associated with poor overall survival in pediatric sarcoma patients, as already reported in melanoma, where it is associated with tumorigenesis, angiogenesis, anchorage-independent growth, and motility [26], and in hepatocellular carcinoma, where it is considered an independent prognostic factor for overall survival and disease-specific recurrence-free survival [48].

Our bioinformatic analysis, conducted using the Xena Genome Browser and multiple public databases, including the TCGA and GTEX datasets, revealed that B4GALNT1 is overexpressed in various solid tumors compared to healthy tissues. Specifically, in paediatric oncogenomic datasets, B4GALNT1 overexpression correlated with poor outcome in OS, RMS, and EWS, this finding highlighting the role of B4GALNT1 as a potential prognostic marker for these cancers.

The analysis of B4GALNT1 expression also correlated with previous data reporting GD2 positive expression in 80% of OS patients [49], 25–100% of RMS [24, 50], 40–90% of EWS [51], and 10–96% of DSRCT patients [50, 52]. We further investigated the prevalence and intensity of GD2 expression in pediatric sarcomas, providing

valuable insights into the potential feasibility of targeting GD2 with CAR T-cell immunotherapy.

Our analysis of fresh tumor biopsies from a cohort of 64 sarcoma patients showed that GD2 was expressed in a substantial proportion of these samples, particularly in OS, ARMS, and DSRCT. The variable expression levels of GD2 across different sarcoma subtypes, combined with our preclinical data, suggest that CAR.GD2 T-cell therapy could be particularly beneficial for patients with high GD2 expression. Indeed, our in vitro studies demonstrated that CAR.GD2 T-cells effectively eradicated GD2-positive sarcoma cells. High GD2-expressing cell lines, such as MG-63, 143B, and U-2OS (OS), were significantly controlled by CAR.GD2 T-cells. The antitumor activity was confirmed by robust cytokine production and real-time tumor cell lysis. However, for sarcoma cell lines with lower GD2 expression, the efficacy of CAR.GD2 T-cells was reduced, although still better as compared to untransduced T cells. These findings indicate that the level of GD2 expression is critical for the efficacy of CAR.GD2 T-cell therapy in sarcomas, highlighting the need for accurate assessment of GD2 levels in tumors before initiating CAR T-cell immunotherapy.

Several drug approaches have been proposed to increase GD2 expression on tumor cells, including the combination of sialic acid and histone deacetylase (HDAC) inhibitors in preclinical models of NBL [53], and an EZH2 inhibitor in EWS [28], SCLC and NSCLC [29], NBL [30] and in medulloblastoma [18]. These approaches selectively and reversibly induce GD2 surface expression, sensitizing tumor cells to effective cytolysis by anti-GD2 CAR T-cells, suggesting that the combinatory use of GD2-modulating drugs and GD2-based CAR T cells could be beneficial also in the context of low GD2-expressing sarcoma. Here, for the first time, we show that also in $GD2^{dim}$ sarcoma cells, such as in OS cell line (HOS) and in ARMS cell lines (RH4. RH41 SCMC), GD2 expression can be upregulated after exposure to the EZH2 inhibitor Tazemetostat, sensitizing tumor cells to the cytotoxic effect of CAR.GD2 T-cells. This suggests a potential synergistic effect between EZH2 inhibitor and CAR.GD2 T-cells also in the context of OS, RMS and EWS.

In multiple in vitro assays, we proved that CAR.GD2 T-cells exert significant antitumor activity against high GD2-expressing sarcomas, particularly RMS and OS, even at very low effector-to-target (E: T) ratios. In stressed co-culture assays, CAR.GD2 T-cells repeatedly exposed to GD2 + ERMS RD cells or OS 143B cells were significantly enriched in TCM and TEM subpopulations for both CD4 + and CD8 + T cell subsets, ensuring a balanced and effective immune response, combining long-term protection with the ability to quickly react to and eliminate tumor cells upon re-exposure.

We also evaluated CAR.GD2 T-cell function in in vivo murine models. In particular, in the metastatic ERMS RD xenograft model, CAR.GD2 T-cells led to significant tumor eradication and prolonged animal survival; in addition, we recorded a persistent expansion of circulating CAR T-cells, with a notable enrichment of the CD8 + CAR + T-cell compartment. However, responses in orthotopic OS mouse models varied. While U-2OS implanted in the tibia showed rapid tumor eradication upon CAR T-cell infusion and increased CAR T-cell expansion, the 143B orthotopic models, despite showing slower tumor growth and improved overall survival, did not achieve complete tumor eradication. These findings underline the complexity of CAR T-cell therapy responses in different tumor microenvironments and models. Previous studies have reported that 143B tumor cells induce the expansion of murine MDSC populations, potentially contributing to resistance to immunotherapy [40]. To overcome this resistance, combinatory approaches, including treatments with all-trans retinoic acid (ATRA), double infusion of third-generation CAR.GD2 T-cells, and IL-7/anti-IL-7 mAb complexes [54] have been explored, though with limited success [40].

In our in vivo study, we sought to investigate the mechanisms underlying the significantly different behaviour of the 143B cell line as compared to other sarcoma models. The primary focus was to determine if the substantial expansion of monocytic and PMN-MDSCs observed with the 143B OS xenograft model could be replicated with other OS lines and the ERMS line. Our findings demonstrate that the expansion of murine MDSCs is indeed restricted to the 143B OS xenograft model. Neither other OS lines (U-2OS, SAOS-2, MG-63, HOS), nor the RD ERMS line induced a significant increase in the MDSC populations in NSG mice. This specificity highlights the unique immunomodulatory capabilities of the 143B OS cell line, making it a critical model for studying the mechanisms responsible for MDSC expansion in the TME.

Secretome analysis provided further insights, revealing that 143B OS cells produce significantly higher amount of G-CSF and CXCL8 compared to other cell lines, both in vitro and in vivo. In particular, while both cytokines were elevated in mice engrafted with 143B cells, only G-CSF appeared essential for MDSC expansion in vivo. Indeed, G-CSF, but not CXCL8, knockout in 143B cells abrogates the expansion of both murine monocytic and PMN-MDSCs in vivo, indicating a more direct or dominant role for G-CSF in this process.

The in vitro human PBMC co-culture experiments corroborated these findings also in a human setting, where 143B cells and their conditioned media induced significant differentiation and expansion of human MDSC subsets, particularly monocytic MDSCs. The absence of G-CSF in 143B knockout-cells led to a marked reduction of this effect, further corroborating the G-CSF central role.

Notably, in the in vitro model of human MDSCs, we were able to confirm that the immunosuppressive environment fostered by 143B cells by increasing the MDSCs, is mediated significantly by G-CSF. Indeed, conditioned media from 143B cells, increasing the percentage of MDSC in culture, did suppress CAR.GD2 T-cell activity, whereas media from G-CSF knockout-cells did not, pointing to the immune evasive strategies deployed by tumors via cytokine secretion. In line with this observation, it has been shown that several tumors expressing high levels of G-CSF are aggressive, more difficult to treat, and present with poor prognosis and high mortality rates [35, 36, 55]. Several studies suggest that G-CSF has a role in tumor-promoting effects on both tumor cells and the TME [36] in colorectal cancers [35, 56], metaplastic breast carcinoma [57], anaplastic thyroid carcinoma [58], pancreatic cancers [59, 60], bladder carcinoma [61] and hepatocellular carcinoma [62]. Indeed, it promotes tumor survival, migration, and stem cell longevity, as well as induces pro-tumorigenic immune cell phenotypes such as M2 macrophages, MDSCs, and regulatory T-cells [63].

Additionally, it has been reported that MDSC were highly enriched in mononuclear cell populations isolated from peripheral blood of G-CSF-mobilized haploidentical donors [64] and they display a marked inhibitory effect in NBL patients treated with CAR.GD2 T-cells [38]. Furthermore, the frequency of circulating PMN-MDSC in NBL patients inversely correlates with the levels of CAR.GD2 T-cells, being more elevated in patients who did not respond or who lost response to the treatment [38]. A recent report has shown that G-CSF derived from OS cells activates the STAT3 signaling pathway, leading to PD-L2 expression on mast cells. These immunosuppressive PD-L2 + mast cells then suppress tumor-specific CD8 + T-cells in a PD-L2-dependent manner [65].

Since we have recapitulated the mechanism of modulating MDSC in the OS model based on the 143B cell line, further studies involving large cohorts of OS patients are needed to validate these findings in a clinical context to corroborate the correlation between G-CSF, and elevated MDSC levels, increased metastasis, heightened aggressiveness, and poor prognosis. Moreover, approaches aimed at neutralizing G-CSF, a key chemokine that not only modulates MDSCs but also enhances Treg activity [63], or directly reducing MDSCs along with other relevant immunosuppressive elements of the TME, such as Tregs and TAMs, could significantly enhance the response to GD2.CAR T-cells.

Overall, our research provides compelling evidence supporting the use of GD2-targeted CAR T-cell therapy for pediatric sarcomas, emphasizing the importance of assessing GD2 expression levels and considering combinatory approaches to overcome resistance mechanisms. Clinical studies are warranted to translate these experimental findings into effective treatment strategies, potentially improving survival outcomes of patients with high GD2-expressing sarcomas.

Methods

Cell lines

The OS cell lines 143B (ATCC-CRL-8303-RRID: CVCL_2270), MG-63 (ATCC-CRL-1427-RRID: CVCL_0426), U-2 OS (ATCC HTB-96-RRID: CVCL_0042), HOS (ATCC CRL-1543), and SAOS-2 (ATCC HTB-85-RRID: CVCL_0548) were obtained from LGC Standards S.r.L, Milano (MI), Italy. The ERMS cell line RD (ATCC CCL136) and the EWS cell lines A-673 (ATCC® CRL-1598-RRID: CVCL_0080) and SK-ES-1 (ATCC HTB86-RRID: CVCL_0627) were obtained from LGC Standards S.r.L, Milano (MI), Italy. The ERMS cell lines SMS-CTR and JR1 cell lines, the ARMS RH4, SCMC and RH30 were kindly provided by Dr R. Rota (Bambino Gesù Children's Hospital, Rome, Italy). Dr Di Giannatale (Bambino Gesù Children's Hospital, Rome, Italy) kindly provided the ERMS cell line CT10. All cell lines were authenticated by STR analysis in the certificated lab "BMR Genomics s.r.l." and tested for mycoplasma every 15 days.

Generation of retroviral vectors

The generation of the clinical grade retroviral vector iCasp9.2A.GD2.CAR-CD28.4–1BBζ has been previously described [12]. In brief, the CAR molecule comprises a single chain variable fragment (scFv) 14.G2a that specifically recognizes the GD2 disialoganglioside. This scFv is cloned in frame with the transmembrane and cytoplasmic costimulatory domain CD28, the costimulatory domain 4.1BB and the CD3-ζ sequence. The vector is designed with a bi-cistronic configuration, which includes the suicide gene inducible Caspase 9 (iC9) separated from the CAR cassette by a 2A sequence. Viral supernatant was generated by the use of the producer cell line 293VEC-RD114 (kindly provided by Dr Caruso, from BioVec Pharma, Canada). An additional retroviral vector encoding eGFP-Firefly-Luciferase (GFP-FF-Luc) was used in selected experiments to label tumor cells for in vitro and in vivo studies.

Genome editing with CRISPR/Cas9 to knockout CXCL8 gene or CSF3 (G-CSF)

CRISPR/Cas9-mediated CXCL8 Knockout (KO) and CRISPR/Cas9-mediated CSF3 KO in 143B cell line was performed using the Alt-R CRISPR-Cas9 System (Integrated DNA Technologies, IDT, USA) through electroporation with the Amaxa 4D-Nucleofector System (Lonza, Basel, Switzerland). In details, the sgRNA was obtained by annealing the crRNA for CXCL8 or CSF3 (Alt-R Cas9 crRNA, IDT), generated from Synthego Design Tool, https://design.synthego.com, and the fluorescently labeled tracrRNA (Alt-R Cas9 tracrRNA-5'ATTO550, IDT) to monitor electroporation efficiency. The CRISPR/Cas9 ribonucleoprotein (RNP) complex was electroporated in 1×10^5 143B cells according to the manufacturer's specifications of 4D-Nucleofector. The targeting sequence for CXCL8 and CSF3 crRNA are listed below: CXCL8 crRNA: CUAAGUUCUUUA GCACUCCU and CSF3 crRNA: AGCUUGUAGGUG GCACACUG.

Isolation and generation of effector T-cells.

Peripheral blood mononuclear cells (PBMCs) were isolated from buffy-coats obtained from healthy donors (Bambino Gesù Children's Hospital, Rome, Italy) who signed a written informed consent, in accordance with rules set by the Institutional Review Board of OPBG (Approval of Ethical Committee N°969/2015 prot. N° 669LB), using Lymphocytes separation medium (Eurobio; France). T lymphocytes were activated with immobilized OKT3 (1 μg/ml, e-Bioscience Inc.;San Diego,CA, USA) and anti-CD28 (1 μg/ml, BD Biosciences, Europe) monoclonal antibody (mAb) in the presence of recombinant human interleukin-7 (IL7, 10 ng/ml; bio-techne; USA) and 15 (IL15, 5 ng/ml; bio-techne; USA). Activated T-cells were then transduced, with the retroviral vector iCasp9.2A.GD2.CAR-CD28.4–1BBζ, on day 3 in 24-well plates pre-coated with recombinant human RetroNectin (Takara-Bio. Inc; Japan) and expanded in vitro for additional 10 days before functional analysis.

Characterization of human MDSC

The frequency and the absolute number of human early (e-MDSC, monocytic (Mo-MDSC and polymorphonuclear (PMN-MDSC) was evaluated by flow-cytometry. For the MDSC characterization, freshly isolated PBMCs were stained with anti-human CD11b-PECy7 (BD-Biosciences: 557,743), HLA-DR-BUV395 (BD-Biosciences: 564,040), CD14-VioBlue (Miltenyi-Biotec: 130-113-714), CD33-PE (BD-Biosciences: 555,450), CD45-BUV805 (BD-Biosciences: 612,891), CD56 APC (BD-Biosciences: 555,518), CD19 APC (BD-Bioscences: 555,415), CD3 APC (BD-Bioscences: 555,342), CD15-BB515 (BD-Bioscences: 565,236) for 15 min at 4 °C and then washed twice with stain buffer (Becton Dickinson). Stained samples were acquired by LSR Fortessa flow-cytometer (Becton Dickinson) and data were analyzed by FlowJo (RRID:SCR_008520) software.

Immunophenotype analysis

GD2 surface expression was analyzed on fresh tumor biopsy samples and PBMC from sarcoma patients using a conjugated mouse anti-human GD2-BV421 monoclonal antibody (clone 14.G2a, BD Biosciences, USA). Cells were stained with a live/dead dye solution, specifically 7-Amino-Actinomycin D (7-AAD) (BD Biosciences, Italy), together with CD45 APC (BD Biosciences, USA). GD2 expression was analyzed in the CD45-negative (CD45-) singlet cell population. In the morphological gate (FSC/SSC) we excluded debris. To ensure consistency and reliability in our analyses, isotype controls and PBMCs as a negative control were included in each flow cytometry run.

CAR.GD2 receptor expression on T-cells was assessed using a specific anti-idiotype primary antibody (1A7) (40), followed by rat anti-mouse kappa PE (BD Biosciences) and analyzed in combination with an anti-CD3-specific monoclonal antibody.

Phenotypic analysis of human T-cells

The following mAbs were used: CD45 (clone HI30, BUV805-Catalog No: 612891), GD2 (clone 14.G2a, BV421-Catalog No: 564223), CD3 (clone SK7, APC-H7-Catalog No: 641415), CD4 (clone SK3, PE-Cy7-Catalog No: 560909), CD8 (clone RPA-T8, BUV395-Catalog No: 563795), CD45RA (clone HI100, APC-Catalog No: 550855), CD62L (clone DREG-56, BV605-Catalog No: 562719) (All from BD Pharmigen, USA). Memory profile of T-cells was determined based on CD62L and CD45RA expression. We considered the following markers to define: *Naïve* T-cells (CD62L + CD45RA +), T Central Memory (TCM; CD62L + CD45RA-), T Effector Memory (TEM; CD62L-CD45RA-), and terminally differentiated effector memory T cells re-expressing CD45RA (TEMRA; CD62L-CD45RA +). The expression of GD2 antigen on tumor cell lines and patient's biopsy tissues was assessed with an anti-GD2 mAb (clone 14.g2a, BD Biosciences, USA). The expression of CAR.GD2 on T-cells was detected using a specific anti-idiotype antibody (1A7) [12]. All antibodies were used as per manufacturer's recommendations. In all the analyses, the population of interest was gated based on forward vs side scatter characteristics followed by singlet gating, and live cells were gated using 7-Amino-Actinomycin D (7-AAD) (BD Biosciences, Italy). Samples were analyzed with a BD LSRFortessa X-20 and Diva software (BD Biosciences). For each sample, a minimum of 20,000 events have been analyzed.

Characterization of murine MDSC

Murine MDSCs were evaluated using anti-murine antibodies to Ly6C (clone HK1.4, eFluor™ 450; eBioscience), Ly6G (clone 1A8; PE-eFluor610; eBioscience), and CD11b (clone M1/70, PE; eBioscience) [40]. All antibodies were used as per manufacturer's recommendations. In all analyses, the population of interest was gated based on forward vs side scatter characteristics followed by singlet gating, and live cells were gated using 7-Amino-Actinomycin D (7-AAD) (BD Biosciences, Italy). Samples were analyzed with a BD LSRFortessa X-20 and Diva software (BD Biosciences). For each sample, a minimum of 20,000 events have been analyzed.

In vitro anti-sarcoma activity

For long-term 5-day co-culture experiments, un-transduced (NT) and iCasp9.2A.GD2.CAR-CD28.4–1BBζ (CAR.GD2) T lymphocytes were plated at 0.5×10^6 cells/well in 24-well plates at the indicated Effector: Target (E:T) ratios. Following 6 days of incubation at 37 °C, adherent tumor cells and T-cells were collected and assessed by fluorescence-activated cell-sorting (FACS) analysis based on CD45 + /CD3 + cells (Effector T-cells) and CD45-GFP + GD2 + (sarcoma tumor $GD2^+$ cell line) or GFP + CD45-GD2- (sarcoma tumor GD2(neg) cell line), respectively.

For "stressed co-cultures assay" [66], tumor cells were added to CAR.GD2 and/or NT T-cells on day 0, 5, 10 and 15 at E:T ratio of 1:1. The residual tumor cells and persisting T-cells were analyzed by FACS analysis, 5 days after each tumor addition (day + 5, day + 10, day + 15 and day + 20).

In the "potency co-culture assay", CAR.GD2 and/or NT T-cells were seeded in 24-well plates at the specified E:T ratios (CAR + T: Tumor) ranging from 1:1 to 1:32. For this experiment, we diluted CAR T-cells in NT-cells while maintaining a fixed final number of both T-cells and tumor cells at 500,000 cells each. After 6 days of incubation at 37 °C, adherent tumor cells and T-cells were harvested and evaluated through FACS analysis.

Treatment of tumor cells with enhancer of zeste homolog 2 inhibitor

The sarcoma cell lines were plated in 6-well plates at a density of 1×10^5 cells per well according our protocol [18]. Tumour cells were treated with the EZH2 inhibitor Tazemetostat (S7128-10MM, Selleck Chemicals, US), dissolved in DMSO at a concentration of 1 or 10 μM or DMSO alone. The cells were incubated at 37 °C and 5% CO_2 for 7 days. The EZH2 inhibitor was replenished at the same concentration when the medium was changed or the cells were split. On day 7 of treatment, the cells were harvested and analysed for GD2 expression.

OS/PBMC conditioned medium

To prepare the OS conditioned medium (CM), $2\times10^4/cm^2$ sarcoma cell lines [(143B, 143B G-CSF knockout (143B G-$CSF^{-/-}$) or U-2OS] were cultured in RPMI supplemented with 10% FBS, 1% Penicillin/Streptomycin and 1% Glutamine (here after Medium). After 72 h (hrs), the conditioned medium (CM_1) was collected, filtered through a 0.4 μm filter, and stored at −20 °C. To prepare CM_2, freshly isolated PBMC ($4\times10^5/cm^2$) were cultures for three days in the OS conditioned medium (CM_1). At the end of the culture, conditioned media (CM_2) were collected, filtered, and stored at −20 °C, and cells were characterized for flow-cytometry. For the negative control, PBMC were cultured in medium for 72 h, conditioned medium (CM_3) was collected, 0.4 μm filtered and stored at −20 °C, whereas the cells were characterized by flow cytometry. For CM_4, freshly isolated PBMC ($4\times10^5/cm^2$) were co-cultured for 72 h with semiconfluent 143B, 143B G-$CSF^{-/-}$ or U-2OS cell line in Medium. At the end of the co-cultures, conditioned media (CM_4) were collected, filtered and stored at −20 °C, whereas the cells were characterized by flow-cytometry.

In selected experiment, PBMC alone or PBMC + 143B G-$CSF^{-/-}$ cells were co-cultured with increasing doses of Human G-CSF, premium grade (Miltenyi; Catalog No: 130-096-347) (ranging from 0.5 to 50 ng/ml) for 72 h. At the end of the co-cultures MDSC were analyzed by flow cytometry.

Real-time incucyte analysis for 2D/3D models

CAR.GD2 T-cell cytotoxic activity was tested by using the IncuCyte S3 live cell imaging system (Sartorius). The GFP + tumor cells were seeded (1,000 cell/well) in an ultra-low-attachment 96-well plate in triplicate. Growth of tumor spheres was daily monitored up to a diameter of 300um and then co-cultured with un-transduced (NT) T-cells or CAR.GD2 T-cells for 5 days at different E:T ratio (1:1, 1:5, 1:10). Spheroid diameter and GFP expression of residual tumor have been analyzed in real time starting 12 h after co-culture up to 120 h (5 days). Moreover, we evaluated cytotoxic activity of CAR.GD2 T-cells on 143B, 143B G-$CSF^{-/-}$ and U-2OS tumor cell lines also in presence of CM_1, CM_2, CM_3 and CM_4. The Incucyte® Live-Cell Analysis Systems was used as real-time quantitative live-cell imaging to monitor cell confluence over time. The Total Green Object Integrated Intensity parameter was used to quantify tumor cells density for five days. The assays were repeated in three independent experiments, and the data were summarized as mean ± Standard Deviation (SD).

Cytokine analysis by Ella automated immunoassay system

The Supernatant was collected 24 h from the in vitro co-culture experiments to measure Interferon gamma

(IFNγ), Interleukin-2 (IL-2), Interleukin-10 (IL-10) and Tumor Necrosis Factor alpha (TNF-α). Supernatant collected, from tumor cell line culture, was collected at 72 h. All Cytokines were quantified by Ella Automated Immunoassay System (bio-techne; Minneapolis, USA).

For the stimulation assays with 1A7 anti-idiotypic antibody, non-transduced (NT) T-cells and CAR.GD2 T-cells were incubated with 0.5 ng/mL of 1A7 anti-idiotypic antibody for 72 h. The 1A7 antibody was used to mimic stimulation by the tumor-associated antigen disialoganglioside GD2. Supernatants were harvested at 24 h post-culture for cytokine analysis, which was performed using an Ella Automated Immunoassay System assay to quantify granulocyte colony-stimulating factor (G-CSF), granulocyte–macrophage colony-stimulating factor (GM-CSF), interferon-gamma (IFNγ), interleukin-6 (IL-6), and interleukin-10 (IL-10) levels.

Cytokine tumor profile analysis by luminex MAGPIX

For in vitro experiments, sarcoma cell lines [RD, 143B, 143B CXCL8 knockout (143B CXCL8$^{-/-}$), 143B G-CSF knockout (143B G-CSF$^{-/-}$), HOS, SAOS-2, U-2OS and MG-63] were plated 1×10^5 cells/ml in 24 well-plate. Supernatant from tumor cultures was collected at 72 h, to measure cytokines release. For in vivo experiments, the murine plasma of xenograft models inoculated with sarcoma cell lines (143B, 143B CXCL8$^{-/-}$, 143B G-CSF$^{-/-}$, U-2OS, MG-63, HOS, SAOS-2 and RD) was collected weekly until mice sacrifice upon reaching log10 bioluminescence value. The plasma of control mice (without tumor) was collected at the same days. Cytokines were measured by Custom Panel assay (Millipore), using a Luminex MAGPIX with xPONENT software, following the manufacturer's instructions. In particular, we investigated the following cytokines: CCL2, CCL3, CCL5, CCL7, CX3CL1, CXCL1, CXCL2, CXCL4, CXCL5, CXCL6, CXCL8 (IL8), CXCL13, CXCL14, G-CSF (CSF3), GM-CSF, IFN-gamma, IL10, IL13, IL1b, IL5, MCSF and TNF-alpha.

Elispot assay

We used an IFNγ ELISpot assay, as described previously [67]. Briefly, CAR T-cells were plated in triplicate, serially diluted from 1×10^6 to 5×10^4 cells/well and then co-cultured with OS primary patient tumors (5×10^4 and 1×10^5 respectively). As positive control, T-cells were stimulated with 25 ng/mL of phorbol myristate acetate (PMA) and 1 µg/mL of ionomycin (Sigma-Aldrich). The IFNγ spot-forming cells (SFC) were enumerated (ZellNet).

In vivo experiments

Xenograft studies were performed using female or male NSG (NOD.Cg-Prkdcscid Il2rgtm1Wjl/SzJ; RRID: BCBC_4611 from Charles River) mice, 6 to 8 weeks of age. To investigate the in vivo antitumor activity of CAR.GD2 T-cells on systemic RMS model, 0.5×10^6 GD2$^+$ RD-GFP-FF-Luc cells were intravenously injected (i.v.). To investigate the in vivo antitumor activity of CAR.GD2 T-cells on orthotopic (o.t.) model of OS, NGS mice were inoculated in the tibia with 0.5×10^6 GD2$^+$ 143B-GFP-FF-Luc or 0.2×10^6 GD2$^+$U-2OS-GFP-FF-Luc. Tumors were injected with matrigel diluted 1:1 in PBS 1X. After tumor engraftment, i.e. when the tumor's bioluminescence was detectable and measurable, the mice received only one *i.v.* injection of effector T-cells (10×10^6/mouse). To investigate which human sarcoma lines modulate mouse MDSC cell expansion, the 143B, SAOS-2, U-2OS, MG-63 and HOS OS cell lines were orthotopically inoculated in the right tibia of NSG mice. For the ERMS model, RD cell line was orthotopically inoculated in the right paw muscle of NSG mice.

Circulating murine MDSC were evaluated periodically in peripheral blood by FACS analysis, as previously reported [40], looking for absolute number of PMN-MDSC (CD11b + Ly6G + Ly6C–) cells and monocytic MDSCs (CD11b + Ly6C +) cells.

Absolute number quantification of PMN MDSC and monocytic MDSCs cells was performed on 50 uL of blood, using CountBright™ Absolute Counting Beads, for flow cytometry kit (Cat# C36950; Invitrogen).

Tumor growth was evaluated using IVIS imaging system (PerkinElmer, USA). Briefly, a constant region of interest was drawn over the mouse and the intensity of the signal measured, every week, as total photon/sec/cm^2/sr (p/s/cm^2/sr), as previously described [68]. The circulating human T-cells were evaluated periodically in mice peripheral blood. Mice were maintained in the animal facility at *Plaisant Castel Romano* (Rome, Italy). All in vivo experiments were performed following the ethical international, EU and national requirements and were approved by the Italian Health Ministry (N°88/2016-PR).

Analysis of public datasets

For the in-silico study, the B4GALNT1 gene expression was evaluated as a prognostic tumor marker and as surrogate marker for GD2 expression level in patients. In particular, the Gene Expression Profiling Interactive Analysis 2 webtool (GEPIA2—Gene Expression Profiling Interactive Analysis (RRID:SCR_018294) (http://gepia2.cancer-pku.cn/) was employed to assess the expression levels of B4GALNT1 across multiple solid tumor types RNAseq data from The Cancer Genome Atlas (TCGA) and the Genotype-Tissue Expression (GTEX) projects. Using Oncogenomics pediatric sarcoma database, we characterize B4GALNT1 gene expression also in pediatric subpopulation.

The Kaplan–Meier survival analysis by B4GALNT1 gene expression have been performed on sarcoma patients using R2 bioinformatic webtool (https://hgserver1.amc.nl/) on publicly available datasets (Oncogenomics, ITCC, Dirksen, TARGET). The cut-off value was automatically calculated for each database based on specific parameters and statistical analysis to maximize the separation between high and low expression groups, allowing the stratification of patients on their molecular profiles.

Statistical analysis

Data are summarized as average ± standard deviation (SD). Student *t*-test (two-sided) or ordinary two-sided one-way ANOVA was used to determine statistically significant differences between samples, with p value < 0.05 indicating a significant difference. Non-parametric matched-pairs statistical tests were used to compare the frequency and the absolute number of MDSC among different culture conditions (Friedman test) or between day 0 and each single condition (Wilcoxon matched-pairs signed-rank test). A p value < 0.05 indicates a significant difference.

Mice were matched based on the tumor signal for control and treated groups. The mouse survival data were analyzed using the Kaplan–Meier survival curves; the log-rank test was used to measure differences between groups. No valuable samples were excluded from the analyses. Animals were excluded only in the event of death after tumor implant, but before T-cell infusion, or for the absence of tumor engraftment. Mice were matched based on the tumor signal for control and treatment groups before infusion of control or gene-modified T-cells. To compare the growth of tumors over time, bioluminescence signal intensity was collected in a blind fashion. Bioluminescence signal intensity was log transformed and then compared using a two-sample t-test. Graph generation and statistical analyses were performed using GraphPad Prism (RRID:SCR_002798) version 10.2.3 software.

Statement of significance

Sarcomas account for 10-15% of all childhood cancers. GD2 expression was detected in approximately 55% of the primary sarcoma tumors and it is positively modulated by EZH2 inhibitor Tazemetostat. Immunosuppressive MDSC hindered the long-term effectiveness of CAR. GD2 T-cells. Tumor-derived G-CSF, but not CXCL8, significantly induces a vigorous expansion of immunosuppressive monocytic MDSC.

Abbreviations

CAR	Chimeric antigen receptor
iC9	Inducible caspase 9
GD2	Disialoganglioside-2
CAR.GD2	CAR.GD2.CD28.4-1BBζ
OPBG	Bambino Gesù children's hospital
eGFP-FFLuc	EGFP-firefly-luciferase
scFv	Single chain variable fragment
PBMC	Peripheral blood mononuclear cells
HD	Healthy donors
IL7	Interleukin-7
IL15	Interleukin-15
IFN-γ	Interferon gamma
TNF-α	Tumor necrosis factor alpha
7-AAD	7-Amino-actinomycin D
1 × PBS	1X phosphate-buffered saline
NSG	NOD/SCID IL-2Rγnull
OS	Osteosarcoma
RMS	Rhabdomyosarcoma
ARMS	Alveolar rhabdomyosarcoma
ERMS	Embryonal rhabdomyosarcoma
EWS	Ewing sarcoma
DSRCT	Desmoplastic small round cell tumors
MDSC	Myeloid-derived suppressor cells
CXCL8	Chemokine (C-X-C motif) ligand 8
G-CSF	Granulocyte colony-stimulating factor
GM-CSF	Granulocyte-macrophage colony-stimulating factor
NBL	Neuroblastoma
B4GALNT1	β-1,4-N-Acetyl-Galactosaminyltransferase 1
MFI	Median fluorescence intensity
SSC	Side scatter
FSC	Forward scatter
TME	Tumor microenvironment
TGCA	The cancer genome atlas
GTEX	Genotype-tissue expression
MFI	Median fluorescence intensity
FSC	Forward scatter

Supplementary Information

The online version contains supplementary material available at https://doi.org/10.1186/s13045-024-01641-7.

Additional file 1
Additional file 2
Additional file 3
Additional file 4
Additional file 5
Additional file 6
Additional file 7
Additional file 8
Additional file 9
Additional file 10
Additional file 11
Additional file 12
Additional file 13
Additional file 14
Additional file 15
Additional file 16
Additional file 17
Additional file 18

Acknowledgements
We are very grateful to BioVec Pharma and Dott. Manuel Caruso in providing the packaging cell line 293Vec-RD114 used for the generation of the retroviral vector used for the manufacturing of CAR.GD2 T-cells. We are very grateful to OPBG Cytometry (in particular, Dr Ezio Giorda, Dr Marco Scarsella and Gabriele Volpe) and Pathology (in particular, Dr Marco Pezzullo and Dr Cristiano De Stefanis) Facilities for supporting our in vitro experiments. We are very grateful to the patients Associations that support our research: Associazione "Raffaele Passarelli" Onlus (B. De Angelis); Associazione "Un…due…tre…Alessio" (C. Quintarelli); Associazione "Famiglia Lazzari" (C. Quintarelli) and Agostino Mazza and family (B. De Angelis).

Author contributions
MP and CQ are the first authors of the paper. BDA and FL are the co-last author of the paper. BDA designed the experimental studies and supervised the project conduction. MP, CQ, BDA and FL analysed the data and wrote the manuscript. MP, CQ, MCQ, AS, SM, LI, AO, RC, AC, MLD, SDC, MS, MG, MA, PDF, RR, SP, MC, V F, ADG, CA, VB, FG and BDA developed the in vitro models and performed the in vitro experiments. MC, MP and VF performed analysis of public datasets. MP, CQ, AS, AO and BDA performed the in vivo experiments. BDA and CQ cloned the retroviral vectors. MS, LI and MP performed FACS analysis; MP performed Incucyte live cell analysis. MP and LI performed cytokines analysis. SM and MCQ performed Genome Editing. ADG, MM, GDB, MB, MB, GM M, FDB and FL provided the patient samples and their expertise to define the clinical translation perspective. BDA, MP, CQ and FL revised the final version of the manuscript. All authors read and approved the final manuscript. The authors declare that the research was conducted in the absence of any commercial or financial relationships that could be construed as a potential conflict of interest.

Funding
The experimental work was supported by grants awarded by: Associazione Italiana Ricerca per la Ricerca sul Cancro Investigator Grant (AIRC-IG ID. 29057) (B. De Angelis); Ricerca Corrente 5X1000 (B. De Angelis); Grant Rete ACC RCR-2022–23682287 Preclinical Models (B. De Angelis). Grants awarded by the Ministry of Health and Alleanza Contro il Cancro-Working Group Sarcoma (ACC-WG Sarcoma) (F. Locatelli); Grants awarded by AIRC-Special Project 5 × 1000 no. 9962 (F. Locatelli); AIRC IG 2018 id. 21724 (F. Locatelli), Ricerca Finalizzata GR-2013–02359212 (C. Quintarelli); Ricerca Corrente (C. Quintarelli). Progetto Ministeriale CAR-T (F. Locatelli); Italian PNRR CN3 "National Center for Gene Therapy and Drugs based on RNA Technology" (F. Locatelli; European Union—Next Generation EU, Mission 4, Component 2, CUP B93D21010860004); LSH-TA Ecosistema innovativo della Salute (F. Locatelli); IMI JU/T2EVOLVE with grant number 945393 (F. Locatelli).

Data availability
All data and Supplemental data associated with this study are presented in the paper. Raw data generated in this study are available upon detailed request to the corresponding authors, upon an agreement signed between the parties for their specific use.

Declarations

Consent for publication
Not applicable.

Competing interests
The authors declare no competing interests.

Author details
[1]Department of Onco-Haematology and Cell and Gene Therapy, Bambino Gesù Children's Hospital, IRCCS, San Paolo N°15 Street, 00146 Rome, Italy. [2]Department of Clinical Medicine and Surgery, Federico II University of Naples, 80131 Naples, Italy. [3]Department of Molecular Medicine, Sapienza University of Rome, 00185 Rome, Italy. [4]PhD Program in Immunology, Molecular Medicine and Applied Biotechnologies, Faculty of Medicine, University of Rome Tor Vergata, 00173 Rome, Italy. [5]Unit of Pathogen Specific Immunity, Bambino Gesù Children's Hospital, IRCCS, 00145 Rome, Italy. [6]Department of Life Sciences and Public Health, Catholic University of the Sacred Heart, S. Onofrio Square, 00165 Rome, Italy.

Received: 11 July 2024 Accepted: 19 November 2024
Published online: 18 December 2024

References

1. Jones DTW, et al. Molecular characteristics and therapeutic vulnerabilities across paediatric solid tumours. Nat Rev Cancer. 2019;19:420–38. https://doi.org/10.1038/s41568-019-0169-x.
2. Dyson KA, et al. Emerging trends in immunotherapy for pediatric sarcomas. J Hematol Oncol. 2019;12:78. https://doi.org/10.1186/s13045-019-0756-z.
3. Hingorani P, et al. Current state of pediatric sarcoma biology and opportunities for future discovery: a report from the sarcoma translational research workshop. Cancer Genet. 2016;209:182–94. https://doi.org/10.1016/j.cancergen.2016.03.004.
4. Thanindratarn P, Dean DC, Nelson SD, Hornicek FJ, Duan Z. Chimeric antigen receptor T (CAR-T) cell immunotherapy for sarcomas: from mechanisms to potential clinical applications. Cancer Treat Rev. 2020;82:101934. https://doi.org/10.1016/j.ctrv.2019.101934.
5. Mensali N, et al. ALPL-1 is a target for chimeric antigen receptor therapy in osteosarcoma. Nat Commun. 2023;14:3375. https://doi.org/10.1038/s41467-023-39097-x.
6. Xiao W, et al. FGFR4-specific CAR-T cells with inducible caspase-9 suicide gene as an approach to treat rhabdomyosarcoma. Cancer Gene Ther. 2024. https://doi.org/10.1038/s41417-024-00823-2.
7. Lake JA, et al. Directing B7–H3 chimeric antigen receptor T cell homing through IL-8 induces potent antitumor activity against pediatric sarcoma. J Immunother Cancer. 2024. https://doi.org/10.1136/jitc-2024-009221.
8. Ahmed N, et al. Human epidermal growth factor receptor 2 (HER2) -specific chimeric antigen receptor-modified T cells for the immunotherapy of HER2-positive sarcoma. J Clin Oncol. 2015;33:1688–96. https://doi.org/10.1200/JCO.2014.58.0225.
9. Hegde M, et al. Tumor response and endogenous immune reactivity after administration of HER2 CAR T cells in a child with metastatic rhabdomyosarcoma. Nat Commun. 2020;11:3549. https://doi.org/10.1038/s41467-020-17175-8.
10. Terry RL, et al. Chimeric antigen receptor T cell therapy and the immunosuppressive tumor microenvironment in pediatric sarcoma. Cancers (Basel). 2021. https://doi.org/10.3390/cancers13184704.
11. Kaczanowska S, et al. Immune determinants of CAR-T cell expansion in solid tumor patients receiving GD2 CAR-T cell therapy. Cancer Cell. 2024. https://doi.org/10.1016/j.ccell.2023.11.011.
12. Quintarelli C, et al. Choice of costimulatory domains and of cytokines determines CAR T-cell activity in neuroblastoma. Oncoimmunology. 2018;7: e1433518. https://doi.org/10.1080/2162402X.2018.1433518.
13. Del Bufalo F, et al. GD2-CART01 for relapsed or refractory high-risk neuroblastoma. N Engl J Med. 2023;388:1284–95. https://doi.org/10.1056/NEJMoa2210859.
14. Schulz G, et al. Detection of ganglioside GD2 in tumor tissues and sera of neuroblastoma patients. Cancer Res. 1984;44:5914–20.
15. Strobel SB, et al. Expression of potential targets for cell-based therapies on melanoma cells. Life (Basel). 2021. https://doi.org/10.3390/life11040269.
16. Majzner RG, et al. GD2-CAR T cell therapy for H3K27M-mutated diffuse midline gliomas. Nature. 2022;603:934–41. https://doi.org/10.1038/s41586-022-04489-4.
17. de Billy E, et al. Dual IGF1R/IR inhibitors in combination with GD2-CAR T-cells display a potent anti-tumor activity in diffuse midline glioma H3K27M-mutant. Neuro Oncol. 2022;24:1150–63. https://doi.org/10.1093/neuonc/noab300.
18. Ciccone R, et al. GD2-targeting CAR T-cell therapy for patients with GD2+ medulloblastoma. Clin Cancer Res. 2024;30:2545–57. https://doi.org/10.1158/1078-0432.CCR-23-1880.
19. Cheresh DA, Rosenberg J, Mujoo K, Hirschowitz L, Reisfeld RA. Biosynthesis and expression of the disialoganglioside GD2, a relevant target

antigen on small cell lung carcinoma for monoclonal antibody-mediated cytolysis. Cancer Res. 1986;46:5112–8.
20. Battula VL, et al. Ganglioside GD2 identifies breast cancer stem cells and promotes tumorigenesis. J Clin Invest. 2012;122:2066–78. https://doi.org/10.1172/JCI59735.
21. Chantada GL, et al. An aggressive bone marrow evaluation including immunocytology with GD2 for advanced retinoblastoma. J Pediatr Hematol Oncol. 2006;28:369–73. https://doi.org/10.1097/00043426-200606000-00009.
22. Modak S, Gerald W, Cheung NK. Disialoganglioside GD2 and a novel tumor antigen: potential targets for immunotherapy of desmoplastic small round cell tumor. Med Pediatr Oncol. 2002;39:547–51. https://doi.org/10.1002/mpo.10151.
23. Kailayangiri S, et al. The ganglioside antigen G(D2) is surface-expressed in Ewing sarcoma and allows for MHC-independent immune targeting. Br J Cancer. 2012;106:1123–33. https://doi.org/10.1038/bjc.2012.57.
24. Saraf AJ, Dickman PS, Hingorani P. Disialoganglioside GD2 expression in pediatric rhabdomyosarcoma: a case series and review of the literature. J Pediatr Hematol Oncol. 2019;41:118–20. https://doi.org/10.1097/MPH.0000000000001311.
25. Yi H, et al. Pan-cancer analysis of B4GALNT1 as a potential prognostic and immunological biomarker. J Immunol Res. 2022;2022:4355890. https://doi.org/10.1155/2022/4355890.
26. Yoshida H, et al. B4GALNT1 induces angiogenesis, anchorage independence growth and motility, and promotes tumorigenesis in melanoma by induction of ganglioside GM2/GD2. Sci Rep. 2020;10:1199. https://doi.org/10.1038/s41598-019-57130-2.
27. Lammie G, Cheung N, Gerald W, Rosenblum M, Cordoncardo C. Ganglioside gd(2) expression in the human nervous-system and in neuroblastomas—an immunohistochemical study. Int J Oncol. 1993;3:909–15. https://doi.org/10.3892/ijo.3.5.909.
28. Kailayangiri S, et al. EZH2 inhibition in ewing sarcoma upregulates G(D2) expression for targeting with gene-modified T cells. Mol Ther. 2019;27:933–46. https://doi.org/10.1016/j.ymthe.2019.02.014.
29. Reppel L, et al. Targeting disialoganglioside GD2 with chimeric antigen receptor-redirected T cells in lung cancer. J Immunother Cancer. 2022. https://doi.org/10.1136/jitc-2021-003897.
30. Mabe NW, et al. Transition to a mesenchymal state in neuroblastoma confers resistance to anti-GD2 antibody via reduced expression of ST8SIA1. Nat Cancer. 2022;3:976–93. https://doi.org/10.1038/s43018-022-00405-x.
31. Alfaro C, et al. Tumor-produced interleukin-8 attracts human myeloid-derived suppressor cells and elicits extrusion of neutrophil extracellular traps (NETs). Clin Cancer Res. 2016;22:3924–36. https://doi.org/10.1158/1078-0432.CCR-15-2463.
32. Jiang H, Wang X, Miao W, Wang B, Qiu Y. CXCL8 promotes the invasion of human osteosarcoma cells by regulation of PI3K/Akt signaling pathway. APMIS. 2017;125:773–80. https://doi.org/10.1111/apm.12721.
33. Liu T, et al. Self-seeding circulating tumor cells promote the proliferation and metastasis of human osteosarcoma by upregulating interleukin-8. Cell Death Dis. 2019;10:575. https://doi.org/10.1038/s41419-019-1795-7.
34. Kowanetz M, et al. Granulocyte-colony stimulating factor promotes lung metastasis through mobilization of Ly6G+Ly6C+ granulocytes. Proc Natl Acad Sci U S A. 2010;107:21248–55. https://doi.org/10.1073/pnas.1015855107.
35. Li W, et al. G-CSF is a key modulator of MDSC and could be a potential therapeutic target in colitis-associated colorectal cancers. Protein Cell. 2016;7:130–40. https://doi.org/10.1007/s13238-015-0237-2.
36. Karagiannidis I, Salataj E, EgalBeswick ESAEJ. G-CSF in tumors: aggressiveness, tumor microenvironment and immune cell regulation. Cytokine. 2021;142:155479. https://doi.org/10.1016/j.cyto.2021.155479.
37. Caforio M, et al. GD2 redirected CAR T and activated NK-cell-mediated secretion of IFNgamma overcomes MYCN-dependent IDO1 inhibition, contributing to neuroblastoma cell immune escape. J Immunother Cancer. 2021. https://doi.org/10.1136/jitc-2020-001502.
38. Tumino N, et al. Polymorphonuclear myeloid-derived suppressor cells impair the anti-tumor efficacy of GD2.CAR T-cells in patients with neuroblastoma. J Hematol Oncol. 2021. https://doi.org/10.1186/s13045-021-01193-0.
39. Quintarelli C, Del Bufalo F, Locatelli F. GD2-CART01 for relapsed or refractory high-risk neuroblastoma. Reply N Engl J Med. 2023;388:2303–4. https://doi.org/10.1056/NEJMc2305296.
40. Long AH, et al. Reduction of MDSCs with all-trans retinoic acid improves CAR therapy efficacy for sarcomas. Cancer Immunol Res. 2016;4:869–80. https://doi.org/10.1158/2326-6066.CIR-15-0230.
41. De Sanctis F, Bronte V, Ugel S. Tumor-induced myeloid-derived suppressor cells. Microbiol Spectr. 2016. https://doi.org/10.1128/microbiolspec.MCHD-0016-2015.
42. Korbecki J, et al. CC chemokines in a tumor: a review of pro-cancer and anti-cancer properties of the ligands of receptors CCR1, CCR2, CCR3, and CCR4. Int J Mol Sci. 2020. https://doi.org/10.3390/ijms21218412.
43. Li BH, Garstka MA, Li ZF. Chemokines and their receptors promoting the recruitment of myeloid-derived suppressor cells into the tumor. Mol Immunol. 2020;117:201–15. https://doi.org/10.1016/j.molimm.2019.11.014.
44. Highfill SL, et al. Disruption of CXCR2-mediated MDSC tumor trafficking enhances anti-PD1 efficacy. Sci Transl Med. 2014. https://doi.org/10.1126/scitranslmed.3007974.
45. Fergusson NJ, Adeel K, Kekre N, Atkins H, Hay KA. A systematic review and meta-analysis of CD22 CAR T-cells alone or in combination with CD19 CAR T-cells. Front Immunol. 2023;14:1178403. https://doi.org/10.3389/fimmu.2023.1178403.
46. Elsallab M, Ellithi M, Hempel S, Abdel-Azim H, Abou-El-Enein M. Long-term response to autologous anti-CD19 chimeric antigen receptor T cells in relapsed or refractory B cell acute lymphoblastic leukemia: a systematic review and meta-analysis. Cancer Gene Ther. 2023;30:845–54. https://doi.org/10.1038/s41417-023-00593-3.
47. Cai F, Zhang J, Gao H, Shen H. Tumor microenvironment and CAR-T cell immunotherapy in B-cell lymphoma. Eur J Haematol. 2024;112:223–35. https://doi.org/10.1111/ejh.14103.
48. Liu W, Chen Y, Yang J, Guo M, Wang L. B4GALNT1 promotes carcinogenesis by regulating epithelial-mesenchymal transition in hepatocellular carcinoma based on pan-cancer analysis. J Gene Med. 2023;25: e3552. https://doi.org/10.1002/jgm.3552.
49. Trautwein NF, et al. First-in-humans PET/MRI of In Vivo GD2 expression in osteosarcoma. J Nucl Med. 2023;64:337–8. https://doi.org/10.2967/jnumed.122.264626.
50. Dobrenkov K, Ostrovnaya I, Gu J, Cheung IY, Cheung NK. Oncotargets GD2 and GD3 are highly expressed in sarcomas of children, adolescents, and young adults. Pediatr Blood Cancer. 2016;63:1780–5. https://doi.org/10.1002/pbc.26097.
51. Spasov NJ, et al. First-line anti-GD2 therapy combined with consolidation chemotherapy in 3 patients with newly diagnosed metastatic ewing sarcoma or Ewing-like sarcoma. J Pediatr Hematol Oncol. 2022;44:e948–53. https://doi.org/10.1097/MPH.0000000000002488.
52. Espinosa-Cotton M, Guo HF, Tickoo SK, Cheung NV. Identification of immunotherapy and radioimmunotherapy targets on desmoplastic small round cell tumors. Front Oncol. 2023;13:1104693. https://doi.org/10.3389/fonc.2023.1104693.
53. van den Bijgaart RJE, et al. Combined sialic acid and histone deacetylase (HDAC) inhibitor treatment up-regulates the neuroblastoma antigen GD2. J Biol Chem. 2019;294:4437–49. https://doi.org/10.1074/jbc.RA118.002763.
54. Martin CE, et al. IL-7/anti-IL-7 mAb complexes augment cytokine potency in mice through association with IgG-Fc and by competition with IL-7R. Blood. 2013;121:4484–92. https://doi.org/10.1182/blood-2012-08-449215.
55. Yokoyama T, et al. Aggressive G-CSF-producing gastric cancer complicated by lung and brain abscesses, mimicking metastases. Gastric Cancer. 2005;8:198–201. https://doi.org/10.1007/s10120-005-0335-6.
56. Yang X, et al. Expression of granulocyte colony stimulating factor receptor in human colorectal cancer. Postgrad Med J. 2005;81:333–7. https://doi.org/10.1136/pgmj.2004.024646.
57. Fukui Y, et al. Granulocyte-colony-stimulating factor-producing metaplastic carcinoma of the breast with significant elevation of serum interleukin-17 and vascular endothelial growth factor levels. Int Cancer Conf J. 2018;7:107–13. https://doi.org/10.1007/s13691-018-0330-5.
58. Fujita T, Ogasawara Y, Naito M, Doihara H, Shimizu N. Anaplastic thyroid carcinoma associated with granulocyte colony-stimulating factor: report of a case. Surg Today. 2006;36:63–7. https://doi.org/10.1007/s00595-005-3100-x.

59. Kitade H, et al. Granulocyte-colony stimulating factor producing anaplastic carcinoma of the pancreas treated by distal pancreatectomy and chemotherapy: report of a case. Surg Case Rep. 2015;1:46. https://doi.org/10.1186/s40792-015-0048-y.
60. Vinzens S, et al. Granulocyte colony-stimulating factor producing anaplastic carcinoma of the pancreas: case report and review of the literature. Anticancer Res. 2017;37:223–8. https://doi.org/10.21873/anticanres.11310.
61. Satoh H, et al. Bladder carcinoma producing granulocyte colony-stimulating factor: a case report. J Urol. 1993;149:843–5. https://doi.org/10.1016/s0022-5347(17)36229-8.
62. Kohno M, et al. Granulocyte colony-stimulating-factor-producing hepatocellular carcinoma with extensive sarcomatous changes: report of a case. Surg Today. 2013;43:439–45. https://doi.org/10.1007/s00595-012-0202-0.
63. Karagiannidis I, et al. G-CSF and G-CSFR induce a pro-tumorigenic macrophage phenotype to promote colon and pancreas tumor growth. Cancers (Basel). 2020. https://doi.org/10.3390/cancers12102868.
64. Tumino N, et al. PMN-MDSC are a new target to rescue graft-versus-leukemia activity of NK cells in haplo-HSC transplantation. Leukemia. 2020;34:932–7. https://doi.org/10.1038/s41375-019-0585-7.
65. Wang C, Lei Z, Zhang C, Hu X. CXCL6-CXCR2 axis-mediated PD-L2(+) mast cell accumulation shapes the immunosuppressive microenvironment in osteosarcoma. Heliyon. 2024;10: e34290. https://doi.org/10.1016/j.heliyon.2024.e34290.
66. Guercio M, et al. CD28.OX40 co-stimulatory combination is associated with long in vivo persistence and high activity of CAR.CD30 T-cells. Haematologica. 2021;106:987–99.
67. Quintarelli C, et al. High-avidity cytotoxic T lymphocytes specific for a new PRAME-derived peptide can target leukemic and leukemic-precursor cells. Blood. 2011;117:3353–62. https://doi.org/10.1182/blood-2010-08-300376.
68. Di Stasi A, De Angelis B, Savoldo B. Gene therapy to improve migration of T cells to the tumor site. Methods Mol Biol. 2010;651:103–18. https://doi.org/10.1007/978-1-60761-786-0_7.

Publisher's Note

Springer Nature remains neutral with regard to jurisdictional claims in published maps and institutional affiliations.